

# LEARNING INTERPRETABLE HIERARCHICAL DYNAMICAL SYSTEMS MODELS FROM TIME SERIES DATA

Manuel Brenner<sup>1,2,\*</sup>, Elias Weber<sup>1,5,\*</sup>, Georgia Koppe<sup>2,3,4,†</sup>, Daniel Durstewitz<sup>1,2,5,†</sup>

<sup>1</sup>Dept. of Theoretical Neuroscience, Central Institute of Mental Health (CIMH),  
Medical Faculty Mannheim, Heidelberg University

<sup>2</sup>Interdisciplinary Center for Scientific Computing, Heidelberg University

<sup>3</sup>Faculty of Mathematics and Computer Science, Heidelberg University

<sup>4</sup>Hector Institute for AI in Psychiatry and Dept. of Psychiatry and Psychotherapy, CIMH

<sup>5</sup>Faculty of Physics and Astronomy, Heidelberg University

{manuel.brenner, daniel.durstewitz}@zi-mannheim.de

<sup>\*</sup>, <sup>†</sup>These authors contributed equally.

## ABSTRACT

In science, we are often interested in obtaining a generative model of the underlying system dynamics from observed time series. While powerful methods for dynamical systems reconstruction (DSR) exist when data come from a single domain, how to best integrate data from multiple dynamical regimes and leverage it for generalization is still an open question. This becomes particularly important when individual time series are short, and group-level information may help to fill in for gaps in single-domain data. At the same time, averaging is not an option in DSR, as it will wipe out crucial dynamical properties (e.g., limit cycles in one domain vs. chaos in another). Hence, a framework is needed that enables to efficiently harvest group-level (multi-domain) information while retaining all single-domain dynamical characteristics. Here we provide such a hierarchical approach and showcase it on popular DSR benchmarks, as well as on neuroscientific and medical time series. In addition to faithful reconstruction of all individual dynamical regimes, our unsupervised methodology discovers common low-dimensional feature spaces in which datasets with similar dynamics cluster. The features spanning these spaces were further dynamically highly interpretable, surprisingly in often linear relation to control parameters that govern the dynamics of the underlying system. Finally, we illustrate transfer learning and generalization to new parameter regimes.

## 1 INTRODUCTION

Foundation models for time series recently blossomed, based on the hope that generalizable temporal features could be extracted from multiple, diverse datasets (Yeh et al., 2023; Miller et al., 2024; Das et al., 2024; Ansari et al., 2024; Rasul et al., 2024). In scientific and medical applications, however, beyond mere time series forecasting, we are often interested in interpretable and mathematically tractable models that can be used to obtain mechanistic insights into the underlying system dynamics. Such models need to be *generative* in a *dynamical systems sense* (Durstewitz et al., 2023), i.e., when simulated, should produce dynamical behavior with the same long-term statistics as the observed system, a property that conventional time series models often lack (Gilpin, 2024). Moreover, accounting for the fact that different time series may be sampled from fundamentally different dynamical regimes, i.e. with different state space topology and attractor structure, may also help to improve generalization and transfer learning (Göring et al., 2024).

This is particularly important in areas like neuroscience (Zeidman et al., 2019) or mental health (Huys et al., 2016; Valton et al., 2020), where the data is not only expensive and difficult to collect (Koppe et al., 2021; Wen et al., 2017), hence comparatively sparse, but also subject to significant variability between individuals or systems (Meyer-Lindenberg, 2023; Fechtelpeter et al., 2024). The challenge in these settings is to develop models that can still identify and exploit commonalities across different datasets while being flexible enough to account for individual differences in dynamical regimes.

Hierarchical models provide a natural solution by separating domain-general and domain-specific features. Such models facilitate the transfer of group-level information across individual datasets (Pan and Yang, 2010), avoiding overfitting and improving generalization to unobserved conditions with minimal data (Kirchmeyer et al., 2022). They further explicitly represent inter-domain variability, as often crucial in addressing scientific hypotheses, by unsupervised extraction of a common feature space within which individual datasets are embedded (Zeidman et al., 2019). While hierarchical modeling is a meanwhile established approach in statistics, including time series analysis (Berliner, 1996; Hyndman et al., 2011), it has so far hardly been applied to the more challenging problem of *dynamical systems reconstruction (DSR)* where we aim for generative models of the system dynamics that can be used for downstream analysis and simulation.

In this work, we propose such a general framework for extracting hierarchical dynamical systems models from multi-domain time series data. Our approach combines low-dimensional, system- or subject-specific parameter vectors with high-dimensional, group-level weights to produce domain-specific recurrent neural networks (RNNs), which can be trained end-to-end using state-of-the-art techniques designed for DSR (Mikhaeil et al., 2022; Hess et al., 2023). Beyond the provision of a common feature space within which all observed systems are embedded, our approach infers system-specific DS models that serve as generative models for the latent processes underlying individual time series observations. We demonstrate the effectiveness of our method in several ways: By integrating data across systems, we enhance model accuracy on multiple short time series (transfer learning). The method further extracts highly interpretable low-dimensional feature spaces from the dynamical systems benchmarks and empirical datasets employed here, including a medical dataset of arterial pulse waves (interpretability). We show how - once a general DSR model has been learned - new models can be inferred that generalize to previously unobserved dynamical regimes with minimal new data (few-shot learning). Finally, we validate our framework on human electroencephalography (EEG) and functional magnetic resonance imaging (fMRI) data, and demonstrate how unsupervised classification in the learned low-dimensional spaces based on *dynamical systems features* profoundly outperforms all other unsupervised detection methods that harvest more ‘conventional’ time series features, providing a strong point for the DSR perspective on time series analysis.

## 2 RELATED WORK

**Dynamical Systems Reconstruction (DSR)** DSR is a rapidly growing field in scientific machine learning. DSR models may be considered a special class of time series (TS) models that, beyond mere TS prediction, aim to learn surrogate models of the data-generating process from TS observations. A proper DSR model needs to preserve the long-term temporal and geometrical properties of the original dynamical system (DS), i.e. its vector field topology and attractor structure, which then enables further scientific analysis (Brunton and Kutz, 2019; Durstewitz et al., 2023; Platt et al., 2023; Gilpin, 2024). A variety of DSR methods have been advanced in recent years, either based on predefined function libraries and symbolic regression, such as Sparse Identification of Nonlinear Dynamics (SINDy; Brunton et al. (2016); Kaiser et al. (2018)), based on Koopman operator theory (Azencot et al., 2020; Brunton et al., 2021; Naiman and Azencot, 2021), on universal approximators such as recurrent neural networks (RNNs; Gajamannage et al. (2023); Brenner et al. (2022); Hess et al. (2023)), reservoir computing (RC; Pathak et al. (2017); Platt et al. (2022; 2023)), or neural ordinary differential equations (Neural ODEs; Chen et al. (2018); Ko et al. (2023)), or on methods that sit somewhere in between universal and domain-specific, like physics-informed neural networks (PINNs; Raissi et al. (2019)). PINNs, like library-based methods, require sufficient domain knowledge to work well in practice (Fotiadis et al., 2023; Subramanian and Mahadevan, 2023; Mouli et al., 2023). To achieve proper reconstruction of a system’s long-term statistics and attractor geometry, often special, control-theoretic training techniques such as sparse or generalized teacher forcing (Brenner et al., 2022; Mikhaeil et al., 2022; Hess et al., 2023) or particular regularization terms that enforce invariant measures (Platt et al., 2023; Jiang et al., 2023; Schiff et al., 2024) are used. Models using these training techniques currently represent the state of the art in this field.

**Hierarchical Time Series and DSR Modeling** Hierarchical models for representing multi-level dependencies or nested groups have a long history in statistics and machine learning (Laird and Ware, 1982; Goldstein, 1987; Gelman and Hill, 2006; McCulloch et al., 2011). The general idea of these approaches is to leverage shared group-level information while accounting for individual-

level variation in an, ideally, interpretable way. Many such frameworks are Bayesian (Allenby et al., 2005; Gelman et al., 2013), informing individual-level distributions by group-level priors, and have been widely applied in psychology and cognitive science (Lee and Wagenmakers, 2013; Kruschke, 2015). In the time series domain, Zoeter and Heskes (2003); Bakker and Heskes (2007), for instance, introduced dynamic hierarchical models that combine individual time series with group-level dependencies. Hierarchical models have also been applied for forecasting chaotic time series (Matsumoto et al., 1998; Hyndman et al., 2011; Xu et al., 2020), or for extracting interpretable summary statistics from time series to capture inter-individual differences (Akintayo and Sarkar, 2018; Yingzhen and Mandt, 2018), for example for clustering dynamical patterns to identify neuron groups with similar response profiles (Lin et al., 2019). Much less work exists in the direction of hierarchical dynamical systems modeling. Roeder et al. (2019) developed a Bayesian framework using variational inference to infer Neural ODE parameters at different hierarchical levels. Yin et al. (2021); Kirchmeyer et al. (2022) used hierarchical models, which decompose dynamics into shared and environment-specific components, to enhance forecasting quality and generalization across different parameter regimes of a DS. Similarly, Bird and Williams (2019) introduced a multi-task dynamical systems model where a latent variable encodes task-specific information for sequence generation across different styles/environments. Inubushi and Goto (2020) and Guo et al. (2021) used reservoir computing for transfer learning between chaotic systems, relying on shared reservoir dynamics without explicitly modeling system-specific dynamics. Finally, Desai et al. (2022) proposed a transfer learning approach for PINNs, fine-tuning only the final layer of a pre-trained model for one-shot learning of ODEs, with the physics-informed component embedding physical priors to reduce the amount of required data.

In all these studies, however, only benchmark systems living in similar dynamical regimes (e.g. all exhibiting periodic orbits) were considered, often only assessing forecasting but not generative performance. This is fundamentally different from the settings with complex, chaotic, topologically diverse dynamics and real-world data we consider here. In particular, we explicitly test the case where different underlying system parameters may tap into *different dynamical regimes* (e.g. periodic vs. non-periodic, chaotic behavior), request our approach to deliver *generative DSR models* that work for all of those regimes, and represent the underlying systems in a common low-dimensional space spanned by *dynamical systems* features.

### 3 METHOD

#### 3.1 HIERARCHIZATION

Assume we have observed multiple, multivariate time series  $\mathbf{x}_{1 \dots T_{\max}^{(j)}}^{(j)}$  of lengths  $T_{\max}^{(j)}$ ,  $j = 1 \dots S$ , such as measurements from related physical systems, from multiple subjects in medical studies (Huys et al., 2016; Valton et al., 2020), or repeated measurements from the same subject across trials (Zeidman et al., 2019). While generally the individual multivariate time series may come from any type of system, in the following we will denote these as ‘subjects’ as our main application examples will be human data. Our main goal is to infer subject-specific DSR models, parameterized by  $\theta_{\text{DSR}}^{(j)}$ , i.e. generative models of the latent dynamics underlying subject-specific observations, approximated by a discrete-time recursive (flow) map of the form

$$\mathbf{z}_t = \mathbf{F}_{\theta_{\text{DSR}}^{(j)}}(\mathbf{z}_{t-1}, \mathbf{s}_t), \quad (1)$$

where  $\mathbf{s}_t$  are possible external inputs (like task stimuli). Observations are related to the dynamical process  $\{\mathbf{z}_t\}$  via some parameterized observation function  $\mathbf{x}_t = h_{\theta_{\text{obs}}^{(j)}}(\mathbf{z}_t)$ . The *differences* between subjects are captured within an ideally low-dimensional parameter space, represented here by learnable subject-specific features  $\mathbf{l}^{(j)} \in \mathbb{R}^{N_{\text{feat}}}$  which are mapped onto the parameters  $\theta_{\text{DSR}}^{(j)}$  of subject-specific DS models through a function parameterized by group-level parameters  $\theta_{\text{group}}$ :

$$\theta_{\text{DSR}}^{(j)} = G_{\theta_{\text{group}}}(\mathbf{l}^{(j)}). \quad (2)$$

The model Eqs. 1-2 is then trained simultaneously on data from all subjects, where features  $\mathbf{l}^{(j)}$  depend only on time series from subject  $j$ . The overall approach is illustrated in Fig. 7. In ablation studies, we explored various ways to parameterize the map  $G_{\theta_{\text{group}}}$ , including flexible and expressive functions like multilayer perceptrons (MLPs) and reparameterizations (see Appx. A.1.3, Table 2), but found that simple linear mappings often gave the best results.

**DSR Model** For our experiments we chose a mathematically tractable (cf. Eisenmann et al. (2024)) RNN model introduced for DSR in Hess et al. (2023), the shallow PLRNN (shPLRNN):

$$\mathbf{z}_t = \mathbf{A}\mathbf{z}_{t-1} + \mathbf{W}_1\phi(\mathbf{W}_2\mathbf{z}_{t-1} + \mathbf{h}_2) + \mathbf{h}_1, \quad (3)$$

with latent states  $\mathbf{z}_t \in \mathbb{R}^M$ , diagonal matrix  $\mathbf{A} \in \mathbb{R}^{M \times M}$ , connectivity matrices  $\mathbf{W}_1 \in \mathbb{R}^{M \times L}$  and  $\mathbf{W}_2 \in \mathbb{R}^{L \times M}$ , and thresholds  $\mathbf{h}_2 \in \mathbb{R}^L$  and  $\mathbf{h}_1 \in \mathbb{R}^M$ , where  $L$  is the dimension of the hidden layer, and rectified-linear-unit nonlinearity  $\phi(\cdot) = \text{ReLU}(\cdot) = \max(0, \cdot)$ .

While our approach is general and can be run with any DSR or TS model, here we spell it out specifically for a hierarchically trained shPLRNN, Eq. 3 (hier-shPLRNN). For this model, the subject-specific DSR model parameters are given by  $\theta_{\text{DSR}}^{(j)} = \{\mathbf{W}_1^{(j)}, \mathbf{W}_2^{(j)}, \mathbf{h}_1^{(j)}, \mathbf{h}_2^{(j)}, \mathbf{A}^{(j)}\}$ . The subject-level parameters  $\theta_{\text{DSR}}^{(j)}$  are obtained from the feature vectors  $\mathbf{l}^{(j)} \in \mathbb{R}^{1 \times N_{\text{feat}}}$  by linearly projecting group-level parameters into the subject space according to:

$$\begin{aligned} \mathbf{A}^{(j)} &:= \text{diag}(\mathbf{l}^{(j)} \cdot \mathbf{P}_A), \quad \mathbf{W}_1^{(j)} := \text{mat}(\mathbf{l}^{(j)} \cdot \mathbf{P}_{W_1}, M, L), \quad \mathbf{W}_2^{(j)} := \text{mat}(\mathbf{l}^{(j)} \cdot \mathbf{P}_{W_2}, L, M), \\ \mathbf{h}_1^{(j)} &:= \mathbf{l}^{(j)} \cdot \mathbf{P}_{h_1}, \quad \mathbf{h}_2^{(j)} := \mathbf{l}^{(j)} \cdot \mathbf{P}_{h_2}, \end{aligned}$$

where  $\text{mat}(\cdot, m, n)$  denotes the operation of reshaping a vector into an  $m \times n$  matrix, and  $\mathbf{P}_{W_1} \in \mathbb{R}^{N_{\text{feat}} \times (M \cdot L)}$ ,  $\mathbf{P}_{W_2} \in \mathbb{R}^{N_{\text{feat}} \times (L \cdot M)}$ ,  $\mathbf{P}_A \in \mathbb{R}^{N_{\text{feat}} \times M}$ ,  $\mathbf{P}_{h_1} \in \mathbb{R}^{N_{\text{feat}} \times M}$ , and  $\mathbf{P}_{h_2} \in \mathbb{R}^{N_{\text{feat}} \times L}$  are group-level parameter matrices learned from all subjects simultaneously. With this, the dynamics of a subject-level shPLRNN, specified through features  $\mathbf{l}^{(j)}$ , is given by:

$$\mathbf{z}_t = \mathbf{A}^{(j)}\mathbf{z}_{t-1} + \mathbf{W}_1^{(j)}\phi(\mathbf{W}_2^{(j)}\mathbf{z}_{t-1} + \mathbf{h}_2^{(j)}) + \mathbf{h}_1^{(j)}, \quad (4)$$

### 3.2 TRAINING METHOD

**Generalized Teacher Forcing (GTF)** For training, we used generalized teacher forcing (GTF) (Hess et al., 2023), a method specifically designed to address exploding gradients, which are known to occur when training DSR models on chaotic time series (Mikhaeil et al., 2022). GTF stabilizes training by linearly interpolating between RNN-generated and data-inferred control states in an optimal way (see Appx. A.1). This method was selected for its state-of-the-art performance across a range of DSR tasks (Hess et al., 2023). As in Hess et al. (2023), we trained directly on the observations, assuming  $\mathbf{x}_t = h_{\theta_{\text{obs}}^{(j)}}(\mathbf{z}_t) = \mathbf{z}_t$  to be the identity mapping. We emphasize that GTF is only used to *train* the model, while at test time the models always run autonomously (i.e., without any feedback from actual observations).

**Batching** During training, we used a batching strategy that ensures each gradient update incorporates data from all subjects. For datasets with a manageable number of subjects, we sampled training sequences  $\mathbf{x}_{1 \dots T_{\text{seq}}}^{(j)}$  from each subject, ensuring that updates reflect the collective dynamics across the entire population. For larger datasets, we sampled a random subset of subjects per batch. We further provided multiple sequences per subject within each minibatch to gather more robust statistics for the subject-specific feature vectors. Losses were then added for each subject-specific minibatch and combined to update both group-level parameters,  $\theta_{\text{group}}$ , and subject-specific feature vectors  $\mathbf{l}^{(j)}$ . We found that a batch size between  $4 - 16 \times$  the number of subjects led to the most robust training and performance (see Sect. A.1.2 and Figs. 8 & 9).

**Differential learning rates** For training we used the RAdam (Liu et al., 2020) optimizer. To ensure successful training, we found it crucial to assign a significantly higher learning rate to the subject-specific feature vectors ( $10^{-3}$ ) than to the group-level matrices ( $10^{-4}$ ). This helped prevent numerical instabilities in the group-level matrices, which occurred with higher learning rates. It also prioritizes the incorporation of subject-specific information through the feature vectors, see Fig. 13.

**Initialization** We used Xavier uniform initialization (Glorot and Bengio, 2010) for the group-level matrices, which is designed to keep the variance of the outputs  $n_{\text{out}}$  of a layer roughly equal to the variance of its inputs  $n_{\text{in}}$  by drawing weights from a uniform distribution in the interval  $[-a, a]$ , where  $a = \sqrt{\frac{6}{n_{\text{in}} + n_{\text{out}}}}$ . We reduced the weights further by a factor of 0.1 to stabilize training. Additionally, we applied  $L_2$  regularization to the group-level matrices to further enhance stability.

**Learnable scaling matrices** Lastly, we introduced a learnable, subject-specific diagonal scaling matrix  $\Sigma$  in order to deal with data that is on different scales across subjects (e.g. for observations of the Lorenz-63 system in the cyclic vs. chaotic regime). This was incorporated by the use of a Gaussian negative log likelihood loss

$$\mathcal{L}(\mathbf{x}_t, \hat{\mathbf{x}}_t) = -\frac{M}{2} \log |\Sigma| - \frac{1}{2} (\mathbf{x}_t - \hat{\mathbf{x}}_t)^T \Sigma^{-1} (\mathbf{x}_t - \hat{\mathbf{x}}_t) + const. \tag{5}$$

in place of the MSE loss suggested in Hess et al. (2023) for training with GTF.

## 4 RESULTS

In the following sections, we highlight various use cases of our hierarchical DSR framework.

### 4.1 TRANSFER LEARNING

To illustrate transfer learning, we used two popular DS benchmarks, where we sampled multivariate time series  $\mathbf{X}^{(j)}$  with varying ground-truth parameters of the underlying ODE systems.

- 1) **Lorenz-63** data consisting of 64 ‘subjects’, simulated by 64 different parameter combinations for the Lorenz-63 model (Lorenz, 1963) of atmospheric convection (Eq. 13), with  $\rho \in \{21, 51, 81, 111\}$ ,  $\sigma \in \{8, 9, 10, 11\}$  and  $\beta \in \{1, 2, 3, 4\}$ .
- 2) **Lorenz-96** data, based on a spatially extended version of the Lorenz model (Lorenz, 1996) with  $N = 10$  dimensions (Eq. 15), consisting of 20 subjects with  $F \in \{10 \cdot (n - 1) + 1\}_{n=1}^{20}$ .

The parameter ranges were chosen to cover multiple dynamical regimes, i.e. with fundamentally different attractor topologies (like limit cycles and chaos, Fig. 1). From each parameter setting, we sampled only short time series ( $T_{\max} = 1000$ ), such that training on individual time series often led to suboptimal outcomes. Thus, leveraging group information was crucial for optimal reconstructions. As established in the field of DSR (Wood, 2010; Durstewitz et al., 2023), we evaluated the quality of reconstruction in terms of how well the reconstructed DS captured the invariant long-term temporal and geometric properties of the ground truth DS: We used a state space divergence  $D_{\text{stsp}}$  to assess geometrical agreement (Koppe et al., 2019; Brenner et al., 2022) and the Hellinger distance  $D_H$  on power spectra (Mikhaeil et al., 2022; Hess et al., 2023) to check temporal agreement between generated and ground truth trajectories (see Appx. A.2).

We compared the performance of our framework to three other recent methods (see Appx. A.4 for details): First, as a baseline we tested an ensemble of individual shPLRNNs, using an otherwise identical training algorithm (a kind of ablation experiment, removing specifically the ‘hierarchical component’). Second, we employed LEarning Across Dynamical Systems (LEADS, Yin et al. (2021)), a framework that trains Neural ODEs for generalizing across DS environments by learning a shared dynamics model jointly with environment-specific models. Third, we trained context-informed dynamics adaptation (CoDA, Kirchmeyer et al. (2022)), an extension of LEADS where parameters of the combined and environment-specific models are drawn from a hypernetwork. As evidenced in Table 1, our hierarchical approach (hier-shPLRNN) *considerably* outperforms all other setups. In fact, competing methods were often not even able to correctly reproduce the long-term attractor dynamics (Appx. Fig. 12), while our approach successfully recovered different attractor topologies (Figs. 1 & 15).

Table 1: Performance of hierarchical and ensemble shPLRNN, CoDA (Kirchmeyer et al., 2022), and LEADS (Yin et al., 2021). Medians (across subjects)  $\pm$  MAD across 10 different training runs.

Dataset	Model	$D_{\text{stsp}}(\downarrow)$	$D_H(\downarrow)$	# params	# shared params
Lorenz-63	hier-shPLRNN	<b>0.394 <math>\pm</math> 0.014</b>	<b>0.097 <math>\pm</math> 0.005</b>	6912	6336
	shPLRNN ensemble	1.82 $\pm$ 0.16	0.118 $\pm$ 0.002	14016	0
	CoDA	1.4 $\pm$ 0.4	0.337 $\pm$ 0.005	97154	96514
	LEADS	9.7 $\pm$ 0.9	0.58 $\pm$ 0.04	8580	132
Lorenz-96	hier-shPLRNN	<b>0.580 <math>\pm</math> 0.002</b>	<b>0.0527 <math>\pm</math> 0.0010</b>	21430	21130
	shPLRNN ensemble	1.291 $\pm$ 0.023	0.0657 $\pm$ 0.0012	42630	0
	CoDA	2.05 $\pm$ 0.07	0.155 $\pm$ 0.003	106647	106447
	LEADS	3.2 $\pm$ 0.5	0.54 $\pm$ 0.06	22575	1075

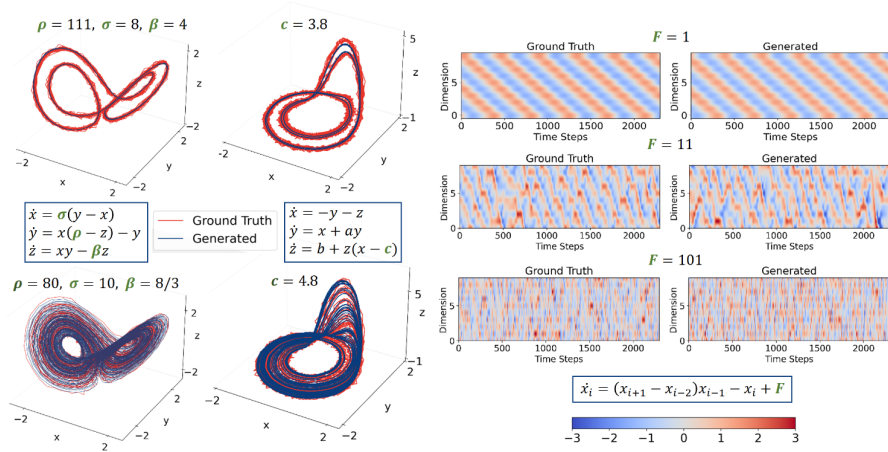


Figure 1: Example reconstructions from a hier-shPLRNN trained on short noisy observations ( $T_{max} = 1000$ , 5% observation noise) from the Lorenz-63, Rössler and Lorenz-96 systems for different  $\{\rho, c, F\}$  (settings as in Sect. 4.1 and 4.2). Shown trajectories were freely generated from a data-inferred initial state, using only subject-specific feature vectors  $\mathbf{l}^{(j)}$  to determine the dynamical regime, and agree in their long-term temporal and geometrical structure with the ground truth (i.e., for times indefinitely beyond the short training sequences).

## 4.2 INTERPRETABILITY

**Dynamical systems benchmarks** We assessed the ability of the hierarchical inference framework to discover interpretable structure from the Lorenz-63 (Eq. 13) and Rössler system (Eq. 14). To this end, we again sampled relatively short time series of length  $T = 1000$  for 10 different values  $\rho^{(j)} \in \{28 \dots 80\}$  for the Lorenz-63, and  $c^{(j)} \in \{3.8 \dots 4.8\}$  for the Rössler, a range where its dynamics undergoes a bifurcation from limit cycle to chaotic dynamics. To reflect these 1-parameter-variation ground truth settings, we also chose  $N_{\text{feat}} = 1$  for the length of the subject-specific parameter vectors. After training, we found that the extracted feature values  $\mathbf{l}^{(j)}$  were highly predictive of the ground truth values for  $\rho^{(j)}$  and  $c^{(j)}$ , with a clearly linear relation (Fig. 2a, see Fig. 17 for the Lorenz-96). The observation that the model automatically inferred such a linear relationship is particularly noteworthy given that the DSR model’s piecewise-linear form (Eq. 4) profoundly differs from the polynomial equations defining the ground truth systems (Eqs. 13 and 14). Surprisingly, even when hier-shPLRNNs were trained with many more features ( $N_{\text{feat}} = 10$ ) than theoretically required, a principal component analysis (PCA) on the feature vectors revealed that a dominant part of the variation was captured by the first PC ( $> 85\%$  of variance), with negligible contributions beyond the third PC (Fig. 2b, blue curve). In contrast, attempts to extract low-dimensional structure from the parameters of individually trained models were unsuccessful, with variation distributed across many PCs (Fig. 2b, gray curve).

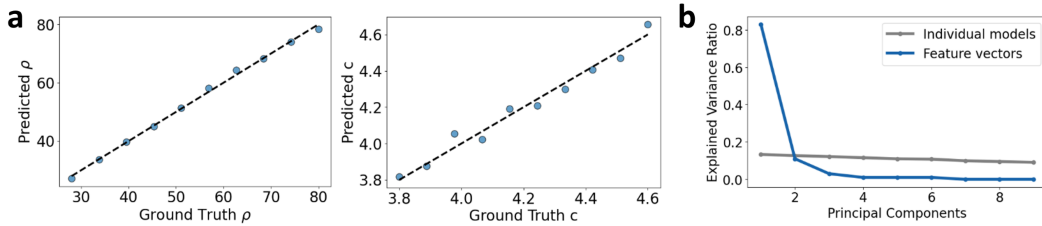


Figure 2: **a**: Analysis of one-dimensional features for hierarchical models trained on observations from the Lorenz-63 (left) and Rössler (right) system for different values of  $\rho$  and  $c$ . **b**: Explained variance ratio of the feature space PCs for a hier-shPLRNN trained on the Lorenz-63 with  $N_{\text{feat}} = 10$  vs. ratio for PCA directly on the parameters of individually trained models.

**Multidimensional parameter spaces** We next examined a scenario where all three of the ground-truth parameters  $\sigma$ ,  $\rho$  and  $\beta$  of the Lorenz-63 (Eq. 13) were jointly varied across a grid of  $4 \times 4 \times 4 = 64$  subjects, as in Sect. 4.1, covering both periodic and chaotic regimes. While naturally, in this case, a scalar subject-specific feature did not capture the full variation in the dataset, we found that good reconstructions could already be achieved using  $N_{\text{feat}} = 3$ , while using  $N_{\text{feat}} = 6$  features led to optimal performance (potentially indicating that for more complex, higher-dimensional scenarios some ‘disentangling’ may be required in feature space to retain linearity in  $G_{\theta_{\text{group}}}$ , Eq. 2, despite the highly nonlinear relation of parameters to dynamics in the ground truth model). The extracted features remained highly interpretable, as illustrated in Fig. 3:  $\rho$  strongly aligned with the first and  $\beta$  with the second PC of the subject feature space, while variation in  $\sigma$  appeared nested within steps of  $\beta$  across PC2. The eight subjects on the left which do not fall into the  $4 \times 4$  grid with the others, correspond to parameter combinations that put the system into a non-chaotic, cyclic regime. These subjects do not only form a distinct group in the first two PCs, but also have significant non-zero third and fourth PCs (see Fig. 16). This observation helps explain why the algorithm benefits from additional features ( $N_{\text{feat}} > 3$ ), as these allow to represent different dynamical regimes as distinct regions in feature space, thereby further supporting its interpretability.

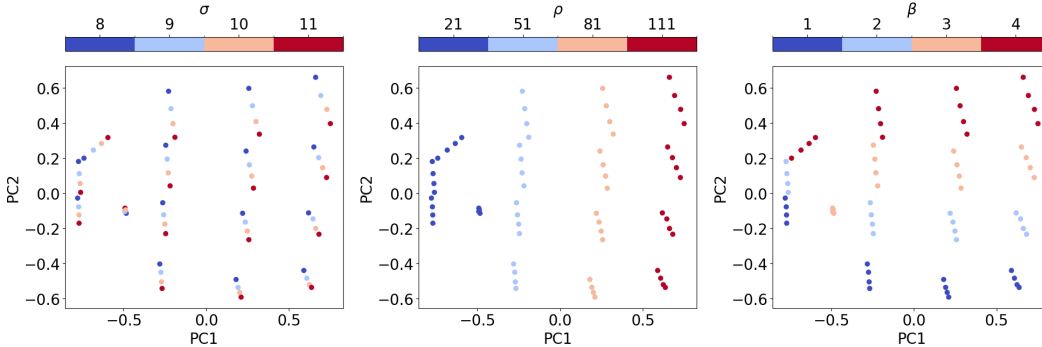


Figure 3: PCA projection of the 6d feature space for a hier-shPLRNN trained on the Lorenz-63 with variation across all 3 ground truth parameters (each dot represents one parameter combination or ‘subject’). From left to right, color-coding corresponds to parameters  $\sigma$ ,  $\rho$  and  $\beta$ , respectively. The learned feature space is highly structured and clearly distinguishes different dynamical regimes.

**Simulated arterial pulse waves** We then tested our approach on a much higher-dimensional ( $N = 52$ ) example system, closer to relevant real-world scenarios, a biophysical model of arterial pulse waves (Charlton et al., 2019). The dataset consists of 4,374 simulated healthy adults aged 25–75 years, with four modalities (pressure, flow velocity, luminal area, and photoplethysmogram) across 13 body sites (see Appx. A.3 for details). Additionally, the dataset includes 32 haemodynamic parameters, such as age, heart rate, arterial size and pulse pressure amplification (Table 4), which specified the biophysical model simulations.

After training, we found that the hier-shPLRNN became an almost perfect emulator of the data, with freely generated trajectories<sup>1</sup> closely matching the ground truth pulse waves (Fig. 4a and Appx. Fig. 18 for further examples). This is particularly impressive given that the number of parameters of the hier-shPLRNN constituted less than 1% of the total amount of training data points, and a comparatively low-dimensional (in relation to the number of biophysical parameters) feature vector ( $N_{\text{feat}} = 12$ ) was sufficient to capture individual differences between subjects. The model’s ability to achieve these reconstructions with so few parameters indicates that it extracted meaningful structure from the data, rather than merely memorizing it. Accordingly, the extracted feature vectors could predict the haemodynamic parameters via linear regression with high – and in all cases statistically significant (F-tests,  $p < 0.05$ ) – accuracy (mean  $R^2 = 0.83$ , Fig. 4b).<sup>2</sup> Two parameters with a particularly strong relationship ( $R^2 > 0.97$ ) are in Fig. 4c. Moreover, the explained variances of the

<sup>1</sup>By freely generated we mean that these are not merely forward predictions, but new trajectories drawn from the generative DSR model using only a data-inferred initial condition.

<sup>2</sup>Further, albeit small improvements in accuracy could be achieved by nonlinear regression via random forests (mean  $R^2 = 0.87$ ).

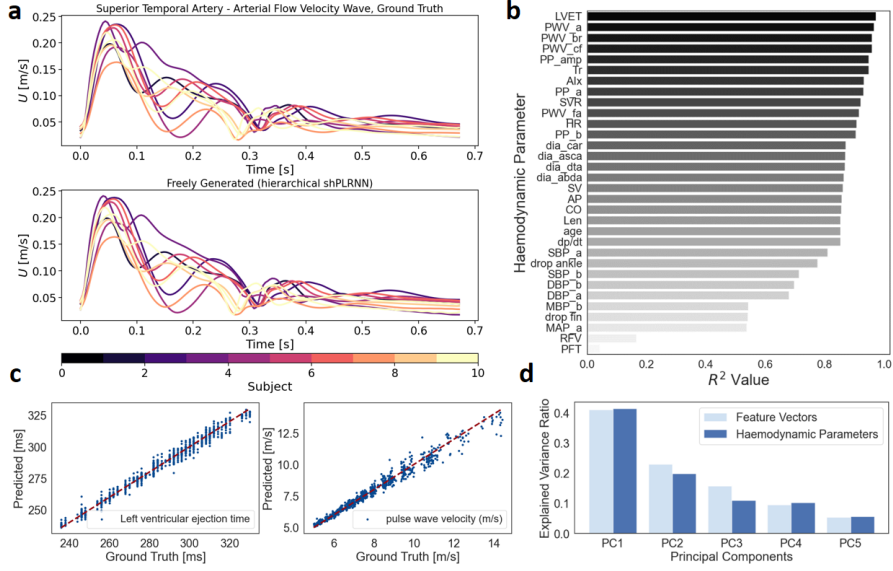


Figure 4: **a:** Ground truth and simulated (freely generated) arterial flow velocity waves for 10 representative subjects (selected by k-medoids, color-coded). **b:**  $R^2$  scores for the 32 ground truth haemodynamic parameters predicted from the learned feature vectors via linear regression. **c:** Ground truth and predicted values for the left ventricular ejection time (LVET) and pulse wave velocity (PWV). **d:** Variance explained by the first 5 principal components of the learned feature space ( $N_{\text{feat}} = 12$ ) and the 32d space spanned by the haemodynamic parameters.

first five principal components of the feature space agreed well with that across the haemodynamic (biophysical) parameter space (Fig. 4d), indicating that the learned feature space accurately captured the pattern of variation in biophysical dynamics. Again, these results are highly non-trivial as the model was trained only on the arterial pulse waves *without any knowledge of the biophysical ground truth parameters*.

### 4.3 FEW-SHOT-LEARNING

To test ‘few-shot learning’, by which we mean here the ability to infer new models from only small amounts of data, we first trained a hier-shPLRNN on  $S = 9$  subjects simulated using the Lorenz-63 with  $\rho_{\text{train}}^{(j)} = \{28, 33.8, 39.6, 45.3, 56.9, 62.7, 68.4, 74.2, 80\}$ . We then generated new, short sequences  $\mathbf{x}_{1 \dots T_{\text{max}}}^{\text{test}}$  with  $T_{\text{max}} = 100$ , using values of  $\rho_{\text{test}}^{(j)}$  randomly sampled from the same interval  $[28, 80]$  that also contained the training data, and fine-tuned only a new feature vector  $\mathbf{l}_{\text{test}}^{(j)}$  on this test set. The model closely approximated (interpolated) the true  $\rho_{\text{test}}^{(j)}$  values from these single short sequences (Fig. 5a), and was even able to *extrapolate* to new  $\rho_{\text{test}}^{(j)}$  outside the training range. Fig. 5b exemplifies how estimates become increasingly robust for longer sequences. This result is noteworthy as training an individual shPLRNN for the Lorenz-63 is challenging even with 1000 time steps (see Table 1 & Fig. 10). Even for sequences as short as  $T_{\text{max}} = 100$ , the loss curves were often uni-modal and smooth around the true parameter values (Fig. 5c), as observed previously for training with sparse or generalized teacher forcing (Hess et al., 2023; Brenner et al., 2024b). This allowed gradient descent to converge rapidly, within 6 seconds on a single 11<sup>th</sup> Gen 2.30 GHz Intel Core i7-11800H. It also enabled efficient use of 2<sup>nd</sup>-order, Hessian-based methods (Newton-Raphson), which converged within just 1 second. Hence, even with minimal data fast and reliable estimation of previously unseen dynamics is feasible, extending into regimes beyond the training domain.

### 4.4 EXPERIMENTS WITH HUMAN EMPIRICAL DATA

**Unsupervised extraction of DS feature spaces from clinical electroencephalogram (EEG) data**  
 In the previous sections, we directly linked extracted feature vectors to known ground truth parameters.



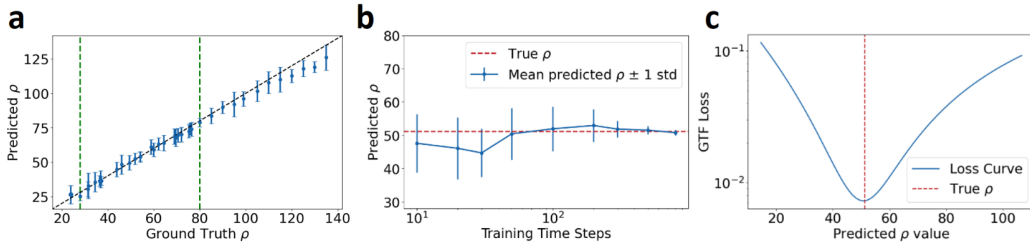


Figure 5: **a**: Predictions (by linear regression as above) for 25  $\rho_{\text{test}}^{(j)}$  values randomly drawn from the training range (green vertical lines) and several  $\rho_{\text{test}}^{(j)}$  values extrapolated beyond the training range, on which only the scalar subject feature ( $N_{\text{feat}} = 1$ ) was fine-tuned on single short test sequences ( $T_{\text{max}} = 100$ ) (see Appx. A.1.5 on how estimates of standard deviation were obtained). **b**: Predictions of a  $\rho^{\text{test}}$  as a function of training sequence length. **c**: GTF loss for a short training sequence ( $T_{\text{max}} = 100$ ) across different values of the scalar subject feature mapped onto  $\rho$  via linear regression. Note the uni-modal loss centered on the true  $\rho^{\text{test}}$  even for this short test set.

However, in most real-world scenarios, ground truth parameters are unavailable and we only have indirect information like class labels, making feature interpretation more challenging. To assess the performance of our hierarchical framework in such settings, we trained it on human EEG data from subjects who were either healthy or experiencing epileptic seizures (Zhang et al., 2022; Andrzejak et al., 2001), as before in a completely *unsupervised* fashion (i.e., ignoring known class labels). Using Gaussian Mixture Models (GMMs) for clustering in the extracted DS feature space, we were able to recover the true class labels with an accuracy of  $92.6 \pm 1.2\%$  across ten runs, *substantially* outperforming several leading approaches for unsupervised feature extraction from time series, such as tsfresh, (Christ et al., 2018), Catch-22, (Lubba et al., 2019), ROCKET (Dempster et al., 2020), MiniRocket (Dempster et al., 2021), and attention-based convolutional autoencoders (Wang et al., 2023) (see Table 5). Fig. 6a shows that the two classes form distinct clusters clearly separated along the first PC of the training data, similar to the clustering of different dynamical regimes in Fig. 3, but unlike the other unsupervised techniques where classes were much less distinct.

Fig. 6b further illustrates *why* mis-classifications happened: The subject shown in the bottom panel is dynamically much more similar to the one shown in the center than the one in the top panel, resulting in similar feature vectors for the center and bottom cases and hence assignment to the same class. An interesting question is why apparently the epileptic subject exhibits seemingly healthy activity, whether for instance there was a labeling error by the experimenter, or whether there is some artifact or electrode misplacement. Unfortunately, we do not have this information, but this case illustrates that even in situations where the class labels are (partially) known, our unsupervised methodology based on similarity in *system dynamics* may reveal interesting information. Taken together, these results demonstrate that our hierarchical framework can automatically discover dynamically relevant features, which allow for the identification of clinically relevant subgroups in an unsupervised way. In particular, our findings confirm that clustering according to DS properties may profoundly improve on ‘classical’ time series feature extraction, as conjectured.

**Transfer learning and classification on human fMRI data** Finally, we tested our hierarchical DSR approach on a set of short fMRI time series from  $2 \times 10$  brain regions from 26 human subjects participating in a cognitive neuroscience experiment (Koppe et al., 2014; 2019), of which 10 with minimal irregularities or artifacts were selected. Based on PCA (Fig. 20c), we determined that a feature vector dimension of  $N_{\text{feat}} = 10$  was necessary to adequately capture the unique characteristics of the individual time series (Fig. 19a). For a left-out subject, reconstruction of the overall dynamics was feasible even when only fine-tuning the low-dimensional feature vector on unseen data (Fig. 19b). Since for this dataset we did not have any ground truth labels or classes, we sought to assess the robustness of feature extraction by computing the cosine similarity matrix across twenty training runs. Strong correlations ( $r \approx 0.85 \pm 0.05$ ) indicated that feature vectors were indeed robustly inferred. Clustering the features via GMMs revealed distinct groups that aligned with visual differences observed in the fMRI time series (Fig. 20).

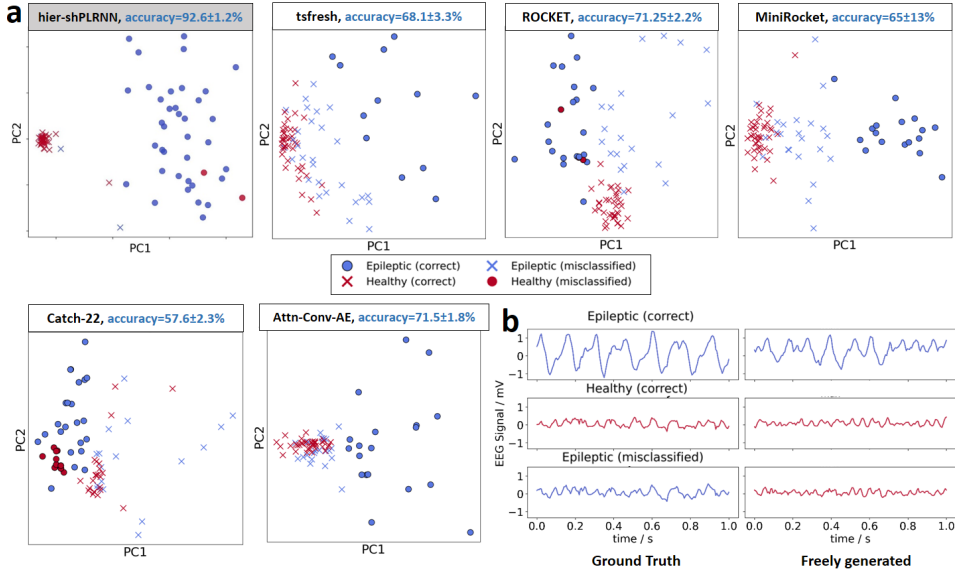


Figure 6: **a**: First two principal components of the embedding spaces of the hier-shPLRNN and other unsupervised time series feature extraction approaches from Table 5. Ground truth labels are indicated by color (blue: epileptic, red: healthy) and predicted labels are indicated by markers (circle: predicted epileptic, cross: predicted healthy). The DS feature space of the hier-shPLRNN exhibits the clearest separation of epileptic and healthy subjects (as confirmed quantitatively). **b**: Left: Ground truth data for two correctly and one incorrectly classified subjects, colored by ground truth labels. Right: Model-generated trajectories, colored by predicted labels.

## 5 CONCLUSIONS

While DSR is currently a burgeoning field, the question of how to best integrate dynamically diverse systems into a common structure, and how to harvest this for transfer learning, generalization, and classification, only recently gained traction (Yin et al., 2021; Kirchmeyer et al., 2022; Göring et al., 2024). Unlike TS models, where the interest lies mainly in forecasting or TS classification/regression, in DSR we aim for generative models that capture invariants of the true, underlying system’s state space. This commonly requires special training algorithms or loss functions (Mikhaeil et al., 2022; Platt et al., 2023). Using GTF (Hess et al., 2023) for training, we demonstrated that hierarchically structured models significantly improve DSR quality and temporal agreement compared to ‘traditional’, non-hierarchical methods. This is a strong indication that our method was able to utilize information from all DS observed, even if located in different dynamical regimes, to boost performance on each individual system. This was confirmed in transfer learning experiments, where models trained on multiple subjects generalized effectively to new conditions with minimal additional data, and did so much more convincingly than various competing methods. Identifying *dynamical regimes*, instead of just utilizing TS waveform features, is also likely to be a more principled approach to TS foundation models, since it is the underlying dynamics which determine a system’s temporal properties across contexts. This idea is supported by the strong classification results on human EEG data, where subject groups were much more clearly segregated in the DS feature space than in spaces constructed by more ‘conventional’ TS models. These DS feature spaces furthermore turned out to be surprisingly interpretable. Extracting these dynamically most crucial features and grouping subjects along these dimensions may be of considerable interest in areas like medicine or neuroscience, and is a new application that has not been considered in the DSR field so far.

**Limitations** The highly interpretable nature of the subject-level feature spaces, despite the strongly nonlinear and chaotic systems considered, is surprising. In future work, it needs to be determined how general this property is and whether it also holds for other physical and biological systems. It appears that our method automatically infers the critical control parameters of a system that best differentiate between dynamical regimes (by controlling the underlying bifurcation structure), but it

is currently unclear what the mathematical basis for this might be. Another potential shortcoming might be that our approach currently is completely unsupervised, while it may be beneficial to use class labels when available. Finally, one useful extension may be a fully Bayesian framework which yields proper posterior uncertainty estimates for parameters.

## REPRODUCIBILITY STATEMENT

Code for this paper is available <https://anonymous.4open.science/r/hier-shPLRNN-5E3C>, and will be made publically available on GitHub with publication at a peer-reviewed journal.

## ACKNOWLEDGEMENTS

This work was funded by the European Union’s Horizon 2020 programme under grant agreement 945263 (IMMERSE), by the Federal Ministry of Science, Education, and Culture (MWK) of the state of Baden-Württemberg within the AI Health Innovation Cluster Initiative and living lab (grant number 31-7547.223-7/3/2), by the German Research Foundation (DFG) within the collaborative research center TRR-265 (project A06 & B08) and Germany’s Excellence Strategy EXC 2181/1 – 390900948 (STRUCTURES), and by the Hector-II foundation.

## REFERENCES

- Adedotun Akintayo and Soumik Sarkar. Hierarchical symbolic dynamic filtering of streaming non-stationary time series data. *Signal Processing*, 151:76–88, October 2018. ISSN 0165-1684. doi: 10.1016/j.sigpro.2018.04.025. URL <https://www.sciencedirect.com/science/article/pii/S0165168418301506>.
- Greg M. Allenby, Peter E. Rossi, and Robert E. McCulloch. Hierarchical Bayes Models: A Practitioners Guide, January 2005. URL <https://papers.ssrn.com/abstract=655541>.
- Ralph G Andrzejak, Klaus Lehnertz, Florian Mormann, Christoph Rieke, Peter David, and Christian E Elger. Indications of nonlinear deterministic and finite-dimensional structures in time series of brain electrical activity: Dependence on recording region and brain state. *Physical Review E*, 64(6):061907, 2001.
- Abdul Fatir Ansari, Lorenzo Stella, Caner Turkmen, Xiyuan Zhang, Pedro Mercado, Huibin Shen, Oleksandr Shchur, Syama Sundar Rangapuram, Sebastian Pineda Arango, Shubham Kapoor, Jasper Zschiegner, Danielle C. Maddix, Michael W. Mahoney, Kari Torkkola, Andrew Gordon Wilson, Michael Bohlke-Schneider, and Yuyang Wang. Chronos: Learning the Language of Time Series, March 2024. URL <http://arxiv.org/abs/2403.07815>. arXiv:2403.07815 [cs].
- Omri Azencot, N. Benjamin Erichson, Vanessa Lin, and Michael W. Mahoney. Forecasting Sequential Data using Consistent Koopman Autoencoders. In *Proceedings of the 37th International Conference on Machine Learning*, 2020. URL <http://arxiv.org/abs/2003.02236>.
- Bart Bakker and Tom Heskes. Learning and approximate inference in dynamic hierarchical models. *Computational Statistics & Data Analysis*, 52(2):821–839, October 2007. ISSN 0167-9473. doi: 10.1016/j.csda.2007.01.001. URL <https://www.sciencedirect.com/science/article/pii/S0167947307000047>.
- L. Mark Berliner. Hierarchical Bayesian Time Series Models. In Kenneth M. Hanson and Richard N. Silver, editors, *Maximum Entropy and Bayesian Methods*, pages 15–22, Dordrecht, 1996. Springer Netherlands. ISBN 978-94-011-5430-7. doi: 10.1007/978-94-011-5430-7\_3.
- Alex Bird and Christopher KI Williams. Customizing sequence generation with multi-task dynamical systems. *arXiv preprint arXiv:1910.05026*, 2019.
- Manuel Brenner, Florian Hess, Jonas M. Mikhaeil, Leonard F. Bereska, Zahra Monfared, Po-Chen Kuo, and Daniel Durstewitz. Tractable Dendritic RNNs for Reconstructing Nonlinear Dynamical Systems. In *Proceedings of the 39th International Conference on Machine Learning*, pages 2292–2320. PMLR, June 2022. URL <https://proceedings.mlr.press/v162/brenner22a.html>. ISSN: 2640-3498.

- Manuel Brenner, Ismail Guennouni, Daniel Durstewitz, Stephanie N. L. Schmidt, Stefanie Lis, Peter Kirsch, and Georgia Koppe. Digital twins of human social interactions reveal behavioral strategies in exchange games, September 2024a. URL <https://osf.io/m6pnq>.
- Manuel Brenner, Florian Hess, Georgia Koppe, and Daniel Durstewitz. Integrating Multimodal Data for Joint Generative Modeling of Complex Dynamics. In *Proceedings of the 41st International Conference on Machine Learning*, pages 4482–4516. PMLR, July 2024b. URL <https://proceedings.mlr.press/v235/brenner24a.html>. ISSN: 2640-3498.
- Steven L Brunton and J Nathan Kutz. *Data-driven science and engineering: Machine learning, dynamical systems, and control*. Cambridge University Press, 2019.
- Steven L. Brunton, Joshua L. Proctor, and J. Nathan Kutz. Discovering governing equations from data by sparse identification of nonlinear dynamical systems. *Proceedings of the National Academy of Sciences USA*, 113(15):3932–3937, 2016. ISSN 0027-8424. doi: 10.1073/pnas.1517384113.
- Steven L. Brunton, Marko Budišić, Eurika Kaiser, and J. Nathan Kutz. Modern Koopman Theory for Dynamical Systems, October 2021. arXiv:2102.12086 [cs, eess, math].
- Peter H. Charlton, Jorge Mariscal Harana, Samuel Vennin, Ye Li, Phil Chowienczyk, and Jordi Alastruey. Modeling arterial pulse waves in healthy aging: a database for in silico evaluation of hemodynamics and pulse wave indexes. *American Journal of Physiology-Heart and Circulatory Physiology*, 317(5):H1062–H1085, November 2019. ISSN 0363-6135. doi: 10.1152/ajpheart.00218.2019. URL <https://journals.physiology.org/doi/full/10.1152/ajpheart.00218.2019>. Publisher: American Physiological Society.
- Ricky TQ Chen, Yulia Rubanova, Jesse Bettencourt, and David K Duvenaud. Neural ordinary differential equations. *Advances in neural information processing systems*, 31, 2018.
- Maximilian Christ, Nils Braun, Julius Neuffer, and Andreas W. Kempa-Liehr. Time Series Feature Extraction on basis of Scalable Hypothesis tests (tsfresh – A Python package). *Neurocomputing*, 307:72–77, September 2018. ISSN 0925-2312. doi: 10.1016/j.neucom.2018.03.067. URL <https://www.sciencedirect.com/science/article/pii/S0925231218304843>.
- Abhimanyu Das, Weihao Kong, Rajat Sen, and Yichen Zhou. A decoder-only foundation model for time-series forecasting, April 2024. URL <http://arxiv.org/abs/2310.10688>. arXiv:2310.10688 [cs].
- Angus Dempster, François Petitjean, and Geoffrey I. Webb. ROCKET: exceptionally fast and accurate time series classification using random convolutional kernels. *Data Mining and Knowledge Discovery*, 34(5):1454–1495, September 2020. ISSN 1573-756X. doi: 10.1007/s10618-020-00701-z. URL <https://doi.org/10.1007/s10618-020-00701-z>.
- Angus Dempster, Daniel F. Schmidt, and Geoffrey I. Webb. MiniRocket: A Very Fast (Almost) Deterministic Transform for Time Series Classification. In *Proceedings of the 27th ACM SIGKDD Conference on Knowledge Discovery & Data Mining, KDD '21*, pages 248–257, New York, NY, USA, August 2021. Association for Computing Machinery. ISBN 978-1-4503-8332-5. doi: 10.1145/3447548.3467231. URL <https://doi.org/10.1145/3447548.3467231>.
- Shaan Desai, Marios Mattheakis, Hayden Joy, Pavlos Protopapas, and Stephen Roberts. One-Shot Transfer Learning of Physics-Informed Neural Networks, July 2022. arXiv:2110.11286 [physics].
- Daniel Durstewitz, Georgia Koppe, and Max Ingo Thurm. Reconstructing computational system dynamics from neural data with recurrent neural networks. *Nature Reviews. Neuroscience*, 24(11): 693–710, November 2023. ISSN 1471-0048. doi: 10.1038/s41583-023-00740-7.
- Lukas Eisenmann, Zahra Monfared, Niclas Göring, and Daniel Durstewitz. Bifurcations and loss jumps in RNN training. *Advances in Neural Information Processing Systems*, 36, 2024.
- Janik Fichtelpeter, Christian Rauschenberg, Hamidreza Jamalabadi, Benjamin Boecking, Therese van Amelsvoort, Ulrich Reininghaus, Daniel Durstewitz, and Georgia Koppe. A control theoretic approach to evaluate and inform ecological momentary interventions, February 2024. Publisher: OSF.

- Stathi Fotiadis, Mario Lino Valencia, Shunlong Hu, Stef Garasto, Chris D. Cantwell, and Anil Anthony Bharath. Disentangled Generative Models for Robust Prediction of System Dynamics. In *Proceedings of the 40th International Conference on Machine Learning*, pages 10222–10248. PMLR, July 2023. URL <https://proceedings.mlr.press/v202/fotiadis23a.html>. ISSN: 2640-3498.
- K. Gajamannage, D. I. Jayathilake, Y. Park, and E. M. Bollt. Recurrent neural networks for dynamical systems: Applications to ordinary differential equations, collective motion, and hydrological modeling. *Chaos*, 33(1):013109, January 2023. ISSN 1054-1500. doi: 10.1063/5.0088748. URL <https://www.ncbi.nlm.nih.gov/pmc/articles/PMC9822653/>.
- Andrew Gelman and Jennifer Hill. *Data Analysis Using Regression and Multilevel/Hierarchical Models*, December 2006. ISBN: 9780511790942 Publisher: Cambridge University Press.
- Andrew Gelman, John B. Carlin, Hal S. Stern, David B. Dunson, Aki Vehtari, and Donald B. Rubin. *Bayesian Data Analysis, Third Edition*. CRC Press, November 2013. ISBN 978-1-4398-4095-5. Google-Books-ID: ZXL6AQAQBAJ.
- William Gilpin. Generative learning for nonlinear dynamics. *Nature Reviews Physics*, 6(3):194–206, March 2024. ISSN 2522-5820. doi: 10.1038/s42254-024-00688-2. URL <https://www.nature.com/articles/s42254-024-00688-2>. Publisher: Nature Publishing Group.
- Xavier Glorot and Yoshua Bengio. Understanding the difficulty of training deep feedforward neural networks. In *Proceedings of the Thirteenth International Conference on Artificial Intelligence and Statistics*, pages 249–256. JMLR Workshop and Conference Proceedings, March 2010. ISSN: 1938-7228.
- Harvey Goldstein. *Multilevel models in education and social research*. Multilevel models in education and social research. Oxford University Press, New York, NY, US, 1987. ISBN 978-0-85264-288-7 978-0-19-520618-0. Pages: viii, 98.
- Yali Guo, Han Zhang, Liang Wang, Huawei Fan, Jinghua Xiao, and Xingang Wang. Transfer learning of chaotic systems. *Chaos: An Interdisciplinary Journal of Nonlinear Science*, 31(1):011104, January 2021. ISSN 1054-1500. doi: 10.1063/5.0033870. URL <https://doi.org/10.1063/5.0033870>.
- Niclas Alexander Göring, Florian Hess, Manuel Brenner, Zahra Monfared, and Daniel Durstewitz. Out-of-Domain Generalization in Dynamical Systems Reconstruction. In *Proceedings of the 41st International Conference on Machine Learning*, pages 16071–16114. PMLR, July 2024. URL <https://proceedings.mlr.press/v235/goring24a.html>. ISSN: 2640-3498.
- Christoph Jürgen Hemmer, Manuel Brenner, Florian Hess, and Daniel Durstewitz. Optimal Recurrent Network Topologies for Dynamical Systems Reconstruction. In *Proceedings of the 41st International Conference on Machine Learning*, pages 18174–18204. PMLR, July 2024. URL <https://proceedings.mlr.press/v235/hemmer24a.html>. ISSN: 2640-3498.
- Florian Hess, Zahra Monfared, Manuel Brenner, and Daniel Durstewitz. Generalized Teacher Forcing for Learning Chaotic Dynamics. In *Proceedings of the 40th International Conference on Machine Learning*, pages 13017–13049. PMLR, July 2023. URL <https://proceedings.mlr.press/v202/hess23a.html>. ISSN: 2640-3498.
- Quentin J. M. Huys, Tiago V. Maia, and Michael J. Frank. Computational psychiatry as a bridge from neuroscience to clinical applications. *Nature Neuroscience*, 19(3):404–413, March 2016. ISSN 1546-1726. doi: 10.1038/nn.4238.
- Rob J. Hyndman, Roman A. Ahmed, George Athanasopoulos, and Han Lin Shang. Optimal combination forecasts for hierarchical time series. *Computational Statistics & Data Analysis*, 55(9): 2579–2589, September 2011. ISSN 0167-9473. doi: 10.1016/j.csda.2011.03.006. URL <https://www.sciencedirect.com/science/article/pii/S0167947311000971>.
- Masanobu Inubushi and Susumu Goto. Transfer learning for nonlinear dynamics and its application to fluid turbulence. *Physical Review E*, 102(4):043301, October 2020. doi: 10.1103/PhysRevE.102.043301. URL <https://link.aps.org/doi/10.1103/PhysRevE.102.043301>. Publisher: American Physical Society.

- Ruoxi Jiang, Peter Y. Lu, Elena Orlova, and Rebecca Willett. Training neural operators to preserve invariant measures of chaotic attractors. *Advances in Neural Information Processing Systems*, 36:27645–27669, December 2023. URL [https://proceedings.neurips.cc/paper\\_files/paper/2023/hash/57d7e7e1593ad1ab6818c258fa5654ce-Abstract-Conference.html](https://proceedings.neurips.cc/paper_files/paper/2023/hash/57d7e7e1593ad1ab6818c258fa5654ce-Abstract-Conference.html).
- E. Kaiser, J. N. Kutz, and S. L. Brunton. Sparse identification of nonlinear dynamics for model predictive control in the low-data limit. *Proceedings of the Royal Society A: Mathematical, Physical and Engineering Sciences*, 474(2219):20180335, November 2018. doi: 10.1098/rspa.2018.0335. Publisher: Royal Society.
- Matthieu Kirchmeyer, Yuan Yin, Jérémie Donà, Nicolas Baskiotis, Alain Rakotomamonjy, and Patrick Gallinari. Generalizing to New Physical Systems via Context-Informed Dynamics Model, June 2022. URL <http://arxiv.org/abs/2202.01889>. arXiv:2202.01889 [cs, stat].
- Joon-Hyuk Ko, Hankyul Koh, Nojun Park, and Wonho Jhe. Homotopy-based training of NeuralODEs for accurate dynamics discovery, May 2023. URL <http://arxiv.org/abs/2210.01407>. arXiv:2210.01407 [physics].
- Georgia Koppe, Harald Gruppe, Gebhard Sammer, Bernd Gallhofer, Peter Kirsch, and Stefanie Lis. Temporal unpredictability of a stimulus sequence affects brain activation differently depending on cognitive task demands. *NeuroImage*, 101:236–244, 2014. ISSN 1095-9572. doi: 10.1016/j.neuroimage.2014.07.008.
- Georgia Koppe, Hazem Toutounji, Peter Kirsch, Stefanie Lis, and Daniel Durstewitz. Identifying nonlinear dynamical systems via generative recurrent neural networks with applications to fMRI. *PLOS Computational Biology*, 15(8):e1007263, 2019. ISSN 1553-7358. doi: 10.1371/journal.pcbi.1007263.
- Georgia Koppe, Andreas Meyer-Lindenberg, and Daniel Durstewitz. Deep learning for small and big data in psychiatry. *Neuropsychopharmacology: Official Publication of the American College of Neuropsychopharmacology*, 46(1):176–190, January 2021. ISSN 1740-634X. doi: 10.1038/s41386-020-0767-z.
- John K. Kruschke. *Doing Bayesian Data Analysis: A Tutorial with R, JAGS, and Stan*. Academic Press, January 2015. ISBN 978-0-12-405888-0. Google-Books-ID: CsOtoAEACAAJ.
- Nan M. Laird and James H. Ware. Random-Effects Models for Longitudinal Data. *Biometrics*, 38(4): 963–974, 1982. ISSN 0006-341X. doi: 10.2307/2529876. URL <https://www.jstor.org/stable/2529876>. Publisher: [Wiley, International Biometric Society].
- Michael D. Lee and Eric-Jan Wagenmakers. *Bayesian cognitive modeling: A practical course*. Bayesian cognitive modeling: A practical course. Cambridge University Press, New York, NY, US, 2013. ISBN 978-1-107-01845-7 978-1-107-60357-8 978-1-107-59612-2. doi: 10.1017/CBO9781139087759. Pages: xiii, 264.
- Alexander Lin, Yingzhuo Zhang, Jeremy Heng, Stephen A Allsop, Kay M Tye, Pierre E Jacob, and Demba Ba. Clustering time series with nonlinear dynamics: A bayesian non-parametric and particle-based approach. In *The 22nd International Conference on Artificial Intelligence and Statistics*, pages 2476–2484. PMLR, 2019.
- Liyuan Liu, Haoming Jiang, Pengcheng He, Weizhu Chen, Xiaodong Liu, Jianfeng Gao, and Jiawei Han. On the variance of the adaptive learning rate and beyond. In *Proceedings of the Eighth International Conference on Learning Representations (ICLR 2020)*, April 2020.
- Edward N Lorenz. Deterministic nonperiodic flow. *Journal of atmospheric sciences*, 20(2):130–141, 1963.
- Edward N Lorenz. Predictability: A problem partly solved. In *Proc. Seminar on predictability*, volume 1, 1996.

- Carl H. Lubba, Sarab S. Sethi, Philip Knaute, Simon R. Schultz, Ben D. Fulcher, and Nick S. Jones. catch22: CAnonical Time-series CHaracteristics. *Data Mining and Knowledge Discovery*, 33(6):1821–1852, November 2019. ISSN 1573-756X. doi: 10.1007/s10618-019-00647-x. URL <https://doi.org/10.1007/s10618-019-00647-x>.
- T. Matsumoto, H. Hamagishi, J. Sugi, and M. Saito. From data-to dynamics: predicting chaotic time series by hierarchical Bayesian neural nets. In *1998 IEEE International Joint Conference on Neural Networks Proceedings. IEEE World Congress on Computational Intelligence (Cat. No.98CH36227)*, volume 3, pages 2535–2540, Anchorage, AK, USA, 1998. IEEE. ISBN 978-0-7803-4859-2. doi: 10.1109/IJCNN.1998.687261. URL <http://ieeexplore.ieee.org/document/687261/>.
- Charles E. McCulloch, Shayle R. Searle, and John M. Neuhaus. *Generalized, Linear, and Mixed Models*. John Wiley & Sons, September 2011. ISBN 978-1-118-20996-7. Google-Books-ID: kyvgyK\_sBlkC.
- Andreas Meyer-Lindenberg. The non-ergodic nature of mental health and psychiatric disorders: implications for biomarker and diagnostic research. *World Psychiatry*, 22(2):272–274, June 2023. ISSN 1723-8617. doi: 10.1002/wps.21086. URL <https://www.ncbi.nlm.nih.gov/pmc/articles/PMC10168159/>.
- Jonas Mikhaeil, Zahra Monfared, and Daniel Durstewitz. On the difficulty of learning chaotic dynamics with RNNs. *Advances in Neural Information Processing Systems*, 35:11297–11312, December 2022. URL [https://proceedings.neurips.cc/paper\\_files/paper/2022/hash/495e55f361708bedbab5d81f92048dcd-Abstract-Conference.html](https://proceedings.neurips.cc/paper_files/paper/2022/hash/495e55f361708bedbab5d81f92048dcd-Abstract-Conference.html).
- John A. Miller, Mohammed Aldosari, Farah Saeed, Nasid Habib Barna, Subas Rana, I. Budak Arpinar, and Ninghao Liu. A Survey of Deep Learning and Foundation Models for Time Series Forecasting, January 2024. URL <http://arxiv.org/abs/2401.13912>. arXiv:2401.13912 [cs].
- S. Chandra Mouli, Muhammad Ashraf Alam, and Bruno Ribeiro. MetaPhysiCa: OOD Robustness in Physics-informed Machine Learning, March 2023. URL <http://arxiv.org/abs/2303.03181>. arXiv:2303.03181 [cs, stat].
- Ilan Naiman and Omri Azencot. A Koopman Approach to Understanding Sequence Neural Models. *arXiv:2102.07824 [cs, math]*, October 2021. URL <http://arxiv.org/abs/2102.07824>.
- Sinno Jialin Pan and Qiang Yang. A Survey on Transfer Learning. *IEEE Transactions on Knowledge and Data Engineering*, 22(10):1345–1359, October 2010. ISSN 1558-2191. doi: 10.1109/TKDE.2009.191. URL <https://ieeexplore.ieee.org/document/5288526>.
- Jaideep Pathak, Zhixin Lu, Brian R. Hunt, Michelle Girvan, and Edward Ott. Using Machine Learning to Replicate Chaotic Attractors and Calculate Lyapunov Exponents from Data. *Chaos: An Interdisciplinary Journal of Nonlinear Science*, 27(12):121102, December 2017. ISSN 1054-1500, 1089-7682. doi: 10.1063/1.5010300. URL <http://arxiv.org/abs/1710.07313>. arXiv: 1710.07313.
- Jason A. Platt, Stephen G. Penny, Timothy A. Smith, Tse-Chun Chen, and Henry D. I. Abarbanel. A Systematic Exploration of Reservoir Computing for Forecasting Complex Spatiotemporal Dynamics, January 2022. URL <http://arxiv.org/abs/2201.08910>. arXiv:2201.08910 [cs].
- Jason A Platt, Stephen G Penny, Timothy A Smith, Tse-Chun Chen, and Henry DI Abarbanel. Constraining chaos: Enforcing dynamical invariants in the training of reservoir computers. *Chaos: An Interdisciplinary Journal of Nonlinear Science*, 33(10), 2023.
- M. Raissi, P. Perdikaris, and G.E. Karniadakis. Physics-informed neural networks: A deep learning framework for solving forward and inverse problems involving nonlinear partial differential equations. *Journal of Computational Physics*, 378:686–707, February 2019. ISSN 00219991. doi: 10.1016/j.jcp.2018.10.045. URL <https://linkinghub.elsevier.com/retrieve/pii/S0021999118307125>.

- Kashif Rasul, Arjun Ashok, Andrew Robert Williams, Hena Ghonia, Rishika Bhagwatkar, Arian Khorasani, Mohammad Javad Darvishi Bayazi, George Adamopoulos, Roland Riachi, Nadhir Hassen, Marin Biloš, Sahil Garg, Anderson Schneider, Nicolas Chapados, Alexandre Drouin, Valentina Zantedeschi, Yuriy Nevmyvaka, and Irina Rish. Lag-Llama: Towards Foundation Models for Probabilistic Time Series Forecasting, February 2024. URL <http://arxiv.org/abs/2310.08278>. arXiv:2310.08278 [cs].
- Geoffrey Roeder, Paul K. Grant, Andrew Phillips, Neil Dalchau, and Edward Meeds. Efficient Amortised Bayesian Inference for Hierarchical and Nonlinear Dynamical Systems. *arXiv:1905.12090 [cs, stat]*, October 2019. URL <http://arxiv.org/abs/1905.12090>. arXiv: 1905.12090.
- O. E. Rössler. An equation for continuous chaos. *Physics Letters A*, 57(5):397–398, 1976. ISSN 0375-9601. doi: 10.1016/0375-9601(76)90101-8. URL <https://www.sciencedirect.com/science/article/pii/0375960176901018>.
- Yair Schiff, Zhong Yi Wan, Jeffrey B. Parker, Stephan Hoyer, Volodymyr Kuleshov, Fei Sha, and Leonardo Zepeda-Núñez. DySLIM: Dynamics Stable Learning by Invariant Measure for Chaotic Systems. In *Proceedings of the 41st International Conference on Machine Learning*, pages 43649–43684. PMLR, July 2024. URL <https://proceedings.mlr.press/v235/schiff24b.html>. ISSN: 2640-3498.
- Abhinav Subramanian and Sankaran Mahadevan. Probabilistic physics-informed machine learning for dynamic systems. *Reliability Engineering & System Safety*, 230:108899, February 2023. ISSN 0951-8320. doi: 10.1016/j.res.2022.108899. URL <https://www.sciencedirect.com/science/article/pii/S0951832022005142>.
- Vincent Valton, Toby Wise, and Oliver J. Robinson. Recommendations for Bayesian hierarchical model specifications for case-control studies in mental health, November 2020. URL <http://arxiv.org/abs/2011.01725>. arXiv:2011.01725 [cs, stat].
- Qixin Wang, Kun Qin, Binbin Lu, Huabo Sun, and Ping Shu. Time-feature attention-based convolutional auto-encoder for flight feature extraction. *Scientific Reports*, 13(1):14175, August 2023. ISSN 2045-2322. doi: 10.1038/s41598-023-41295-y. URL <https://www.nature.com/articles/s41598-023-41295-y>. Publisher: Nature Publishing Group.
- Cheng K Fred Wen, Stefan Schneider, Arthur A Stone, and Donna Spruijt-Metz. Compliance With Mobile Ecological Momentary Assessment Protocols in Children and Adolescents: A Systematic Review and Meta-Analysis. *Journal of Medical Internet Research*, 19(4):e132, April 2017. ISSN 1439-4456. doi: 10.2196/jmir.6641. URL <https://www.ncbi.nlm.nih.gov/pmc/articles/PMC5425774/>.
- Simon N. Wood. Statistical inference for noisy nonlinear ecological dynamic systems. *Nature*, 466(7310):1102–1104, August 2010. ISSN 1476-4687. doi: 10.1038/nature09319. URL <https://www.nature.com/articles/nature09319>. Number: 7310 Publisher: Nature Publishing Group.
- Meiling Xu, Min Han, C. L. Philip Chen, and Tie Qiu. Recurrent Broad Learning Systems for Time Series Prediction. *IEEE Transactions on Cybernetics*, 50(4):1405–1417, April 2020. ISSN 2168-2275. doi: 10.1109/TCYB.2018.2863020. URL <https://ieeexplore.ieee.org/document/8458240>. Conference Name: IEEE Transactions on Cybernetics.
- Chin-Chia Michael Yeh, Xin Dai, Huiyuan Chen, Yan Zheng, Yujie Fan, Audrey Der, Vivian Lai, Zhongfang Zhuang, Junpeng Wang, Liang Wang, and Wei Zhang. Toward a Foundation Model for Time Series Data, October 2023. URL <http://arxiv.org/abs/2310.03916>. arXiv:2310.03916 [cs].
- Yuan Yin, Ibrahim Ayed, Emmanuel de Bézenac, Nicolas Baskiotis, and Patrick Gallinari. LEADS: Learning Dynamical Systems that Generalize Across Environments. In *Advances in Neural Information Processing Systems*, volume 34, pages 7561–7573. Curran Associates, Inc., 2021. URL <https://proceedings.neurips.cc/paper/2021/hash/3df1d4b96d8976ff5986393e8767f5b2-Abstract.html>.



Li Yingzhen and Stephan Mandt. Disentangled sequential autoencoder. In *International Conference on Machine Learning*, pages 5670–5679. PMLR, 2018.

Peter Zeidman, Amirhossein Jafarian, Mohamed L. Seghier, Vladimir Litvak, Hayriye Cagnan, Cathy J. Price, and Karl J. Friston. A guide to group effective connectivity analysis, part 2: Second level analysis with PEB. *NeuroImage*, 200:12–25, October 2019. ISSN 1095-9572. doi: 10.1016/j.neuroimage.2019.06.032.

Xiang Zhang, Ziyuan Zhao, Theodoros Tsiligkaridis, and Marinka Zitnik. Self-supervised contrastive pre-training for time series via time-frequency consistency, 2022. URL <https://arxiv.org/abs/2206.08496>.

O. Zoeter and T. Heskes. Hierarchical visualization of time-series data using switching linear dynamical systems. *IEEE Transactions on Pattern Analysis and Machine Intelligence*, 25(10): 1202–1214, October 2003. ISSN 1939-3539. doi: 10.1109/TPAMI.2003.1233895. URL <https://ieeexplore.ieee.org/document/1233895>.

## A METHODOLOGICAL DETAILS

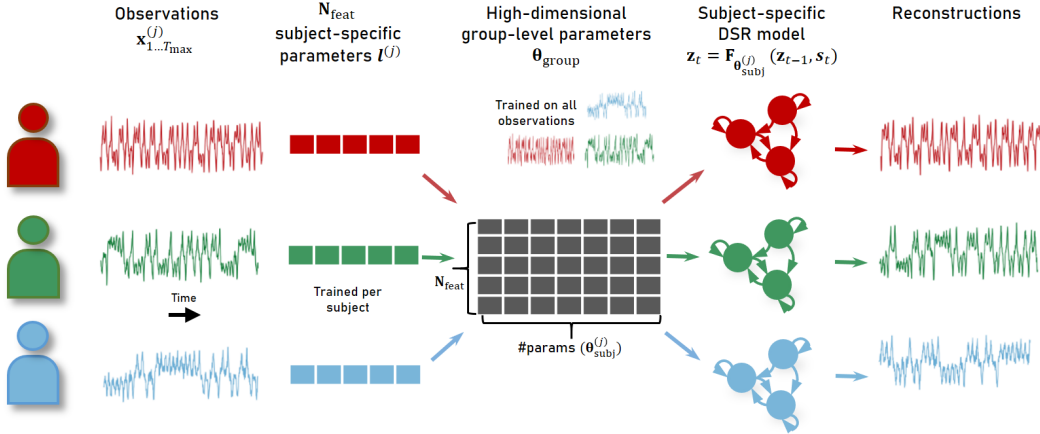


Figure 7: Illustration of the hierarchization framework.

### A.1 MODEL TRAINING

#### A.1.1 GENERALIZED TEACHER FORCING (GTF)

GTF interpolates between forward-propagated latent states  $z_t$  of the DSR model and states  $\tilde{z}_t = h^{-1}(x_t)$  inferred from the observations according to:

$$\tilde{z}_t := (1 - \alpha)z_t + \alpha\tilde{z}_t, \tag{6}$$

with  $0 \leq \alpha \leq 1$ , which may be set by line search or adaptively adjusted throughout training. [Hess et al. \(2023\)](#) prove that an optimal choice for  $\alpha$  leads to bounded gradients as sequence length  $T$  goes to infinity. An extension of GTF to multimodal and non-Gaussian data (multimodal teacher forcing, MTF) has recently been proposed ([Brenner et al., 2024b](#)), and applied to short multi-subject non-Gaussian time series ([Brenner et al., 2024a](#)). MTF can be naturally incorporated into our hierarchical framework and hence is an interesting avenue for further applications.

#### A.1.2 BATCHING

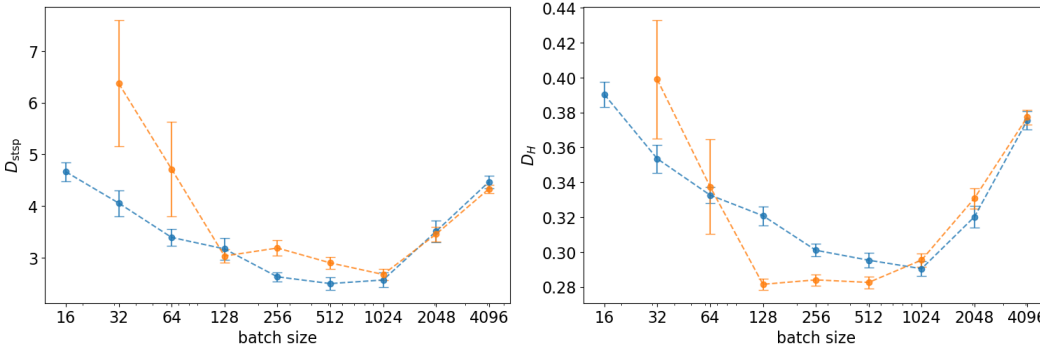


Figure 8: Mean reconstruction performance for different batch sizes (error bars = standard deviation). The blue curve corresponds to training with a fixed number of gradient steps per epoch, while the orange curve represents training with a fixed amount of data per epoch. Some models with smaller batch sizes failed to train entirely, leading to high variance for batch sizes 32 and 64 and the exclusion of batch size 16.

Given the complexity of the datasets considered here, an optimal batching strategy for stochastic optimization is not obvious a priori. We hence investigated how different batch sizes impact the

reconstruction performance of models trained on the 64-subject Lorenz-63 dataset (see main text). The blue curve in Fig. 8 illustrates how performance varies across a range of batch sizes when training with 50 batches per epoch, corresponding to a fixed number of gradient updates per epoch. In this setup, models trained with smaller batch sizes naturally see less data per epoch than those with larger batches. To ensure that the observed effects are not merely due to reduced data exposure with smaller batch sizes, we repeated the experiment using the same batch sizes, but ensuring the entire dataset was seen in each epoch (orange curve). Our findings suggest that smaller batch sizes do not contain enough statistical information across all subjects, leading to higher variance in gradient updates and, in some cases, failure of training. For larger batch sizes, the performance difference was marginal.

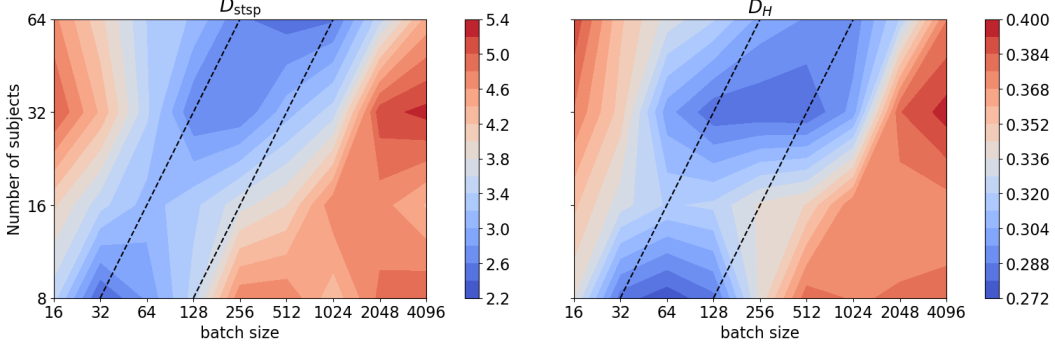


Figure 9: Reconstruction performance for different batch sizes and numbers of subjects. The optimal batch size ranges approximately between  $4\text{--}16 \times$  the number of subjects, as highlighted by the dashed black lines.

The previous experiments were conducted with a fixed number of subjects. However, since we aim to incorporate information from all subjects within each batch, we extended the analysis to examine how the optimal batch size scales with different numbers of subjects. To do this, we randomly sampled smaller subsets from the dataset and repeated the experiment. Fig. 9 gives a heat map of the results, showing that the optimal batch size falls between 4 and 16 times the number of subjects in the dataset. For datasets with a large number of subjects, this range becomes computationally infeasible, so we instead sample batch sequences from a random subset of subjects on each iteration.

### A.1.3 HIERARCHIZATION SCHEME

As discussed in Sect. 1, our hierarchization framework is flexible, allowing for different forms of the group-level function  $G_{\theta_{\text{group}}}$  that maps subject-specific feature vectors to model weights. Here we discuss different choices for parameterizing  $G_{\theta_{\text{group}}}$  and points to consider in this context. The naive approach, employing direct linear projections, results in over-parameterization. For example, the weight matrices  $\mathbf{W}_1$  and  $\mathbf{W}_2$  of the shPLRNN have  $M \times L$  degrees of freedom, but when parameterized with feature vectors through  $\mathbf{W}_1^{(j)} := \text{mat}(\mathbf{l}^{(j)} \cdot \mathbf{P}_{W_1}, M, L)$ , the number of trainable parameters expands to  $N_{\text{feat}} \times (M \times L + 1)$ , which with  $N_{\text{feat}} > 1$  exceeds the  $M \times L$  available entries in  $\mathbf{W}_1$ .

To address this, we tested using outer product forms, reducing parameter load by constructing all subject-specific weight matrices from two matrices  $\mathbf{P}_{W_1} \in \mathbb{R}^{M \times N_{\text{feat}}}$  and  $\mathbf{Q}_{W_1} \in \mathbb{R}^{N_{\text{feat}} \times L}$  via:

$$\mathbf{W}_1^{(j)} = \mathbf{P}_{W_1} \text{diag}(\mathbf{l}^{(j)}) \mathbf{Q}_{W_1} \quad (7)$$

(analogously for  $\mathbf{W}_2$ ), while the diagonal of  $\mathbf{A}$  and vectors  $\mathbf{b}_1, \mathbf{b}_2$  were specified directly through linear maps. This reduces the number of parameters to  $N_{\text{feat}} \times (M + L + 1)$ . In the cases where  $N_{\text{feat}} < M$ , such that the matrices would not be full rank, we applied an extra step to map the feature vector to an auxiliary vector  $\mathbb{R}^M \ni \mathbf{a}^{(j)} = \mathbf{R} \mathbf{l}^{(j)}$  via the shared<sup>3</sup> matrix  $\mathbf{R} \in \mathbb{R}^{M \times N_{\text{feat}}}$ , and subsequently mapped to the weights  $\mathbf{W}_1^{(j)} = \mathbf{P}_{W_1} \text{diag}(\mathbf{a}^{(j)}) \mathbf{Q}_{W_1}$  (analogously for  $\mathbf{W}_2$ ). We also tested using an MLP for mapping the feature vectors onto the subject-specific DSR model weights,

<sup>3</sup>To avoid increasing the number of free parameters,  $\mathbf{R}$  could also be chosen to be random and constant.

with MLP parameters shared among subjects:

$$\theta_{\text{DSR}}^{(j)} = \text{MLP}(\mathbf{l}^{(j)}) \tag{8}$$

The MLP mapped onto a flat vector, which was reshaped into the respective shPLRNN weight matrices.

Both of these schemes did, however, not significantly improve reconstruction results on the Lorenz-63 dataset (see Sect. 4.1) when compared to the naive linear approach according to one-sided t-tests, see Tab. 2.

Table 2: Median state space divergence and Hellinger distance for different parameterizations of the hierarchization scheme, for 10 models each trained on the 64 subjects created via the Lorenz-63 system. The MLP parameterization was clearly inferior, while the linear and outer product approaches were statistically indistinguishable.

Scheme	# params	$D_{\text{stsp}}$			$D_H$		
		Value ( $\downarrow$ )	t(18)	p	Value ( $\downarrow$ )	t(18)	p
Naive linear	6912	$0.394 \pm 0.014$			$0.097 \pm 0.005$		
Outer product	3348	$0.36 \pm 0.03$	0.99	16%	$0.0986 \pm 0.0025$	-0.63	73%
MLP	36713	$0.85 \pm 0.09$	-7.55	100%	$0.111 \pm 0.004$	-5.54	100%

#### A.1.4 DATASET SIZE

To further evaluate the robustness of our approach, we conducted additional experiments on the Lorenz-63 dataset as in Sect. 4.1, but with a varying number of time steps for each subject/system, where 1000 training time steps corresponds to the setting in Sect. 4.1. Fig. 10 shows the ratio between the hierarchical model’s performance and the baseline performance (with values below 1 indicating superior performance by the hierarchical model). Even for long training sequences the hierarchical model consistently outperforms the baseline, particularly in terms of state-space divergence.

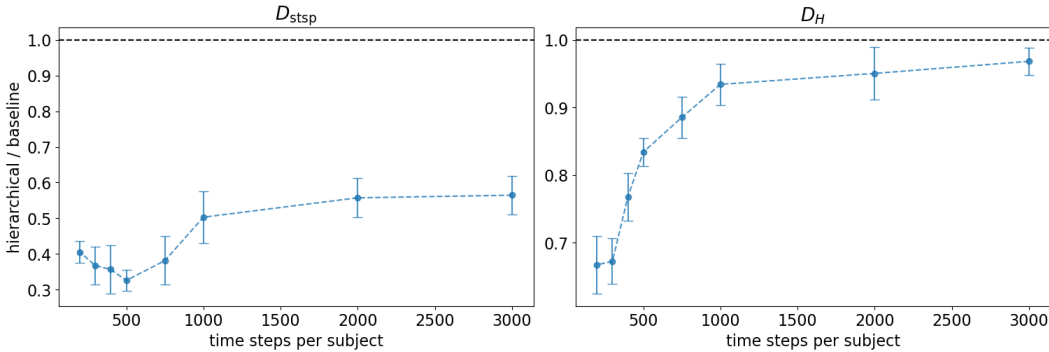


Figure 10: Relative performance (hierarchical/baseline) as a function of time series length for the 64-subject Lorenz-63 dataset.

#### A.1.5 UNCERTAINTY ESTIMATES

To obtain the uncertainty estimates (error bars) in Figs. 5b and c, we first drew a long trajectory with 10000 time steps from the ground truth system using  $\rho^{(S+1)}$ . We then randomly sampled multiple training subsequences of length  $T_{\text{max}}$ , inferred the feature vectors  $\hat{\mathbf{l}}^{(S+1)}$  for each subsequence individually, and calculated the standard deviation of the resulting  $\hat{\rho}^{(S+1)}$  estimates. As shown in Fig. 11, the estimates sharpen as longer training sequences are used.

#### A.1.6 HYPERPARAMETERS

In Tab. 3 we report the hyperparameters used for training the shPLRNN models on the datasets in Sect. 4.1. These include the latent dimension  $M$  (equivalent to the dimension of the observed data),

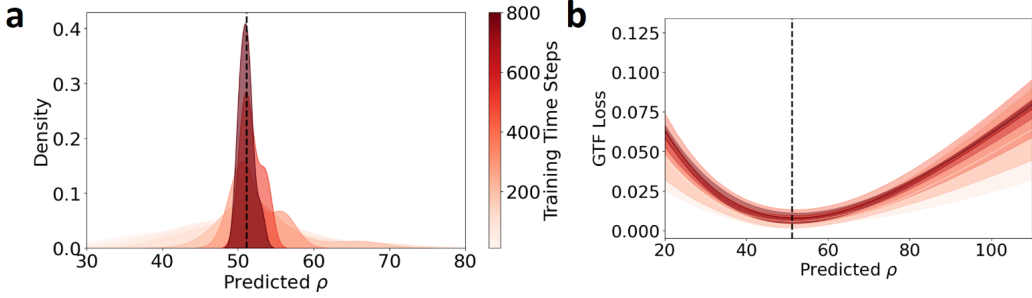


Figure 11: **a**: Distributions  $p(\hat{\rho}^{(j)} | \mathbf{x}_{1 \dots T_{\max}}^{(j)})$  (approximated using kernel density estimates), estimated from 10 time series each with length with different lengths  $T_{\max}$  (color-coded) for the example  $\rho_{\text{test}}^{(j)}$  from Fig. 5. **b**: Corresponding GTF loss curves for different training sequence lengths, illustrating that longer sequences/more training data lead to smaller standard deviation over loss curves.

the hidden dimension  $L$ , the GTF interpolation strength  $\alpha$ , as well as the number of features  $N_{\text{feat}}$ . As recommended in Hess et al. (2023),  $\alpha$  decays exponentially from  $\alpha_{\text{start}}$  at the beginning to  $\alpha_{\text{end}}$  at the end of training.

Table 3: Hyperparameters for our models from Sect. 4.1.

Benchmark	Model	$N_{\text{feat}}$	$M$	$L$	$\alpha_{\text{start}}$	$\alpha_{\text{end}}$
Lorenz-63	shPLRNN ensemble	-	3	30	0.2	0.02
	hier-shPLRNN	6	3	150	0.2	0.02
Lorenz-96	shPLRNN ensemble	-	10	100	0.2	0.02
	hier-shPLRNN	5	10	200	0.2	0.02

## A.2 EVALUATION MEASURES

**State Space Divergence**  $D_{\text{stsp}}$  is the Kullback-Leibler divergence between generated,  $p_{\text{gen}}(x)$ , and ground truth,  $p_{\text{true}}(x)$ , trajectory point distributions in state space (hence a measure of geometrical similarity):

$$D_{\text{stsp}} = KL(p_{\text{gen}} \| p_{\text{true}}) = \int p_{\text{gen}}(x) \log \frac{p_{\text{gen}}(x)}{p_{\text{true}}(x)} dx \quad (9)$$

In lower dimensional state spaces this may be approximated by discrete binning: Let  $m$  be the number of bins in each dimension and  $\hat{p}^{(k)}$  the number of points in the  $k$ -th bin, then with a total number of bins  $N = m^d$ , an estimate of the state space divergence is given by

$$D_{\text{stsp}} \simeq \sum_{k=1}^N \hat{p}_{\text{gen}}^{(k)}(x) \log \frac{\hat{p}_{\text{gen}}^{(k)}(x)}{\hat{p}_{\text{true}}^{(k)}(x)} \quad (10)$$

Since the total number of bins scales exponentially with the observation dimension  $N$ , for experiments with the Lorenz-96 system, we used  $m = 5$  per dimension, as suggested in Hemmer et al. (2024), to ensure the approach remained computationally feasible. For very high-dimensional spaces, Brenner et al. (2022); Mikhaeil et al. (2022) suggest a GMM-based estimate with Gaussians centered on the trajectory points (which was not required here, however). For the values in Table 1, we sampled single time series with 10,000 time steps from both the ground truth system (serving as the test set) and from each trained model, inferring only the initial state from the first time step of the test set, and cutting off transients (1,000 time steps) to focus on the long term attractor behavior.

**Average Hellinger Distance** To assess long-term temporal agreement, we calculated the average Hellinger distance  $D_H$  between the power spectra of true and generated time series (Mikhaeil et al., 2022). Let  $f_i(\omega)$  be the power spectrum for the  $i$ -th dimension (time series variable), then the

Hellinger distance averaged across all dimensions is defined as

$$D_H = \frac{1}{d} \sum_{i=1}^d \sqrt{1 - \int \sqrt{f_i^{(\text{true})}(\omega) f_i^{(\text{gen})}(\omega)} d\omega} \quad (11)$$

The respective power spectra are estimated by the Fast Fourier Transform (FFT), which leads to the integral approximation

$$D_H \simeq \frac{1}{d} \sum_{i=1}^d \sqrt{1 - \sum_j \sqrt{f_i^{(\text{true})}(\omega_j) f_i^{(\text{gen})}(\omega_j)}} \quad (12)$$

Test set and model-generated trajectories were computed as for  $D_{\text{stsp}}$ .

### A.3 DATASETS

**Lorenz-63 system** The famous 3d chaotic Lorenz attractor (Lorenz, 1963) is probably the most widely used benchmark system in DSR. Its governing equations are given by:

$$\begin{aligned} \dot{x} &= \sigma(y - x), \\ \dot{y} &= x(\rho - z) - y, \\ \dot{z} &= xy - \beta z. \end{aligned} \quad (13)$$

Standard parameter settings putting the system into a chaotic regime are  $\sigma = 10$ ,  $\rho = 28$ , and  $\beta = 8/3$ . We further included a Gaussian observation noise term, adding 5% of the subject-specific data variance to each time series  $x_{1 \dots T_{\max}}^{(j)}$ .

**Rössler system** The chaotic Rössler system (Rössler, 1976) is defined by:

$$\begin{aligned} \dot{x} &= -y - z, \\ \dot{y} &= x + ay, \\ \dot{z} &= b + z(x - c). \end{aligned} \quad (14)$$

Standard parameter settings that place the system in a chaotic regime are  $a = 0.2$ ,  $b = 0.2$ , and  $c = 5.7$ . As for the Lorenz-63, we included a Gaussian observation noise term with 5% of the subject-specific data variance.

**Lorenz-96 system** The Lorenz-96 is an extension of the Loren-63 system to an arbitrary number of spatial dimensions  $N$ , introduced in Lorenz (1996). The governing equations are defined by

$$\dot{x}_i = (x_{i+1} - x_{i-2})x_{i-1} - x_i + F \quad (15)$$

with  $x_{-1} = x_{N-1}$ ,  $x_0 = x_N$ ,  $x_{N+1} = x_1$ , and a forcing parameter  $F$ . Again, we added Gaussian observation noise with 5% of the subject-specific data variance.

Trajectories for all three benchmark systems were generated by numerically integrating the ODEs using an implementation of a 4<sup>th</sup>-order Runge-Kutta solver in `scipy.integrate` with a step size of  $\Delta t = .01$ .

**Pulse Wave Dataset** The pulse wave dataset (Charlton et al., 2019) was taken from <https://peterhcharlton.github.io/pwdb/>. It consists of pulse wave time series, simulated for 4,374 healthy adults aged 25–75 years, at 13 common arterial sites within the cardiovascular system (AorticRoot, ThorAorta, AbdAorta, IliacBif, Carotid, SupTemporal, SupMidCerebral, Brachial, Radial, Digital, CommonIliac, Femoral, AntTibial). For each site, four physiological quantities (Arterial Pressure Wave, Arterial Flow Velocity Wave, Arterial Luminal Area Wave, and Photoplethysmogram Wave) were simulated. This resulted in a total of 52 simulated pulse waves (4 quantities recorded at 13 sites) per virtual subject. The dataset further contains 32 hemodynamic parameters used for

Abbreviation	Parameter
age	Age, in years
HR	Heart rate (HR), in beats per minute (bpm)
SV	Stroke volume (SV), in millilitres (ml)
CO	Cardiac output (CO), in litres per minute (L/min)
LVET	Left ventricular ejection time (LVET), in milliseconds (ms)
dp/dt	Max. value of first derivative of the aortic root pressure wave (mmHg/s)
PFT	Time of peak flow at aortic root, in milliseconds (ms)
RFV	Reverse flow volume at aortic root, in millilitres (ml)
SBP	Systolic blood pressure, in mmHg
DBP	Diastolic blood pressure, in mmHg
MBP	Mean blood pressure, in mmHg
PP	Pulse pressure, in mmHg
PP_amp	Pulse pressure amplification, a ratio of brachial to aortic PP
AP	Augmentation pressure at the carotid artery, in mmHg
AIx	Augmentation index at the carotid artery, %
Tr	Time to reflected wave at carotid artery, in ms
PWV_a	Pulse wave velocity (m/s) measured between the aortic root and iliac bifurcation
PWV_cf	Pulse wave velocity (m/s) measured between the carotid and femoral arteries
PWV_br	Pulse wave velocity (m/s) measured between the brachial and radial arteries
PWV_fa	Pulse wave velocity (m/s) measured between the femoral and anterior tibial (ankle) arteries
dia_asca	Ascending aorta diameter (mm)
dia_dta	Descending thoracic aorta diameter (mm)
dia_abda	Abdominal aorta diameter (mm)
dia_car	Carotid diameter (mm)
len	Length of proximal aorta (mm)
drop_fin	MBP drop from aortic root to digital artery, in mmHg
drop_ankle	MBP drop from aortic root to anterior tibial artery, in mmHg
SVR	Systemic vascular resistance ( $\times 10^6$ Pa s / m <sup>3</sup> )

Table 4: The 32 ground truth haemodynamic parameters for the pulse wave dataset (Charlton et al., 2019). Descriptions taken from [https://github.com/peterhcharlton/pwdb/wiki/pwdb\\_haemod\\_params.csv](https://github.com/peterhcharlton/pwdb/wiki/pwdb_haemod_params.csv).

simulating the subject’s pulse waves, listed in Table 4. The parameter PFT (time of peak flow at the aortic root) was nearly constant (78 for 124 subjects and 80 for all other subjects) and hence omitted from our regression analysis. For training, we standardized the time series subject- and dimension-wise, since some time series featured significant differences between subjects in their first moment, particularly in the Arterial Luminal Area Waves (possibly overriding some of the more relevant DS features as evidenced in lower training performance).

**Human EEG Data** The EEG recordings from epileptic patients and healthy controls were originally provided in Andrzejak et al. (2001) and reformatted by Zhang et al. (2022). The dataset is publicly available on the Time Series Classification Website (<https://www.timeseriesclassification.com/description.php?Dataset=Epilepsy2>) under ‘Epilepsy2’. The original set contains 500 single-channel EEG measurements, recorded for 23.6s at 174Hz. These were then split into 1s sequences, which were labeled as displaying either epileptic or healthy activity. From these sequences, 80 (40 per class) were selected as the training set on the Time Series Classification Website, which we used for our experiments. We further standardized the data with a global mean and standard deviation across all subjects in order to retain the relative amplitudes of the sequences.

#### A.4 COMPARISON METHODS

**Selection of comparisons** The approaches by Roeder et al. (2019), Yin et al. (2021) and Kirchmeyer et al. (2022) are the most sensible benchmarks for our study, as they address both forecasting and generalization across different parameter settings of DS. Yin et al. (2021) and Kirchmeyer et al. (2022) were directly evaluated in our work, while Roeder et al. (2019) was excluded due to their focus on short-term dynamical responses with relatively simple dynamics, and the integration of prior knowledge. Inubushi and Goto (2020) and Guo et al. (2021) do not learn subject-specific models or focus solely on shared dynamics, limiting their relevance for DSR. For Bird and Williams (2019), the primary focus was not on DSR but rather on generating sequences in specific styles using a multi-task DS. Further, no code was publicly available. Desai et al. (2022), on the other hand, requires strong physical priors, making it less suitable for our benchmarks, which focus on more general, data-driven methods.

**LEADS** The LEADS (LEarning Across Dynamical Systems, (Yin et al., 2021)) framework decomposes the dynamics model into shared and environment-specific components. For each environment  $e \in E$ , the dynamics are modeled as a linear combination of shared dynamics  $f$  and environment-

specific dynamics  $g_e$ :

$$f_e(x) = f(x) + g_e(x), \quad (16)$$

where  $f$  captures common dynamics across environments, and  $g_e$  models the individual characteristics of environment  $e$ . The learning objective is to minimize the complexity of the environment-specific terms  $g_e$  while ensuring accurate modeling of the overall system dynamics. This is achieved by solving the following optimization problem:

$$\min_{f, \{g_e\}_{e \in E}} \sum_{e \in E} \Omega(g_e) \quad \text{subject to} \quad \forall x_t^e, \frac{dx_t^e}{dt} = f(x_t^e) + g_e(x_t^e) \quad (17)$$

where  $\Omega(g_e)$  is a regularization term that penalizes the complexity of the environment-specific terms.

We used the implementation of LEADS provided by the authors on their public GitHub page (<https://github.com/yuan-yin/LEADS>). For both the Lorenz-63 and Lorenz-96 benchmarks described in Sect. 4.1, we scanned different sequence lengths (`seq_len`  $\in \{5, 10, 20, 30\}$ ), using a fixed time step `dt` = 0.01 and adjusting `num_traj_per_env` to provide the same number of training time steps per environment/setting as for the other methods. We used the `Forecaster` net with the ‘mlp’ setting and a hidden dimension of 6/20 (for Lorenz-63/96) to ensure approximately the same number of parameters as for the hier-shPLRNN. We used the default learning rate of  $lr = 1.e - 3$  as employed for all experiments in Yin et al. (2021), and scanned `lambda_inv`  $\in \{5.e - 4, 1.e - 4, 1.e - 5\}$  and `factor_lip`  $\in \{1.e - 2, 1.e - 3, 1.e - 4\}$ . Despite hyperparameter tuning, LEADS struggled to capture the long-term dynamics of both the Lorenz-63 and Lorenz-96 systems. Models either converged to simple fixed points or exhibited unstable and divergent behavior for long-term forecasts. Given that performance metrics cannot be computed for divergent trajectories, the results presented here are hence for models predicting fixed point dynamics after short transients locally fitting the dynamics.

**CoDA** As in LEADS, in CoDA (Context-Informed Dynamics Adaptation, Kirchmeyer et al. (2022)) the dynamics for each environment  $e \in E$  is modeled as a combination of shared dynamics  $f$  and environment-specific dynamics. However, here the environment-specific dynamics are modeled via a low-dimensional context vector  $\xi_e$  that is used to generate environment-specific dynamics through a hypernetwork:

$$f_e(x) = f(x) + W\xi_e \quad (18)$$

where  $W$  is a learned weight matrix. As for LEADS, the learning objective is to minimize the contribution of the context vectors  $\xi_e$  while ensuring accurate modeling of the individual system dynamics. This is achieved by solving the following optimization problem:

$$\min_{f, W, \{\xi_e\}_{e \in E}} \sum_{e \in E} (L(f(x) + W\xi_e) + \lambda \|\xi_e\|^2), \quad (19)$$

where  $\lambda \|\xi_e\|^2$  is a regularization term. We used the implementation of CoDA provided on the authors’ GitHub site (<https://github.com/yuan-yin/CoDA>). The architecture is fixed, allowing only to change the various regularization coefficients as hyperparameters. For those we scanned similar values as the authors in their experiments,  $\lambda_\xi \in \{1.e - 2, 1.e - 3, 1.e - 4\}$ ,  $\lambda_{\ell_1} \in \{1.e - 5, 1.e - 6, 1.e - 7\}$ ,  $\lambda_{\ell_2} \in \{1.e - 5, 1.e - 6, 1.e - 7\}$ , and  $\dim(\xi) \in \{3, 6, 10\}$ . While overall working much better than LEADS, CoDA was still less reliable in recovering the long-term properties of the underlying systems than our method. Fig. 12 illustrates this for an example subject trained on the Lorenz-63, where the power spectrum learned by CoDA is much less accurate, especially in the low-frequency range.

## A.5 UNSUPERVISED FEATURE EXTRACTION

**tsfresh** We used the Python implementation of `tsfresh` (Christ et al., 2018), which automatically extracts a large set of time series features and selects the most relevant ones for further analysis.

**Catch-22** Catch-22 is a collection of 22 time series features that are both informative and computationally efficient (Lubba et al., 2019). We used the default implementation from the `tslearn` package.



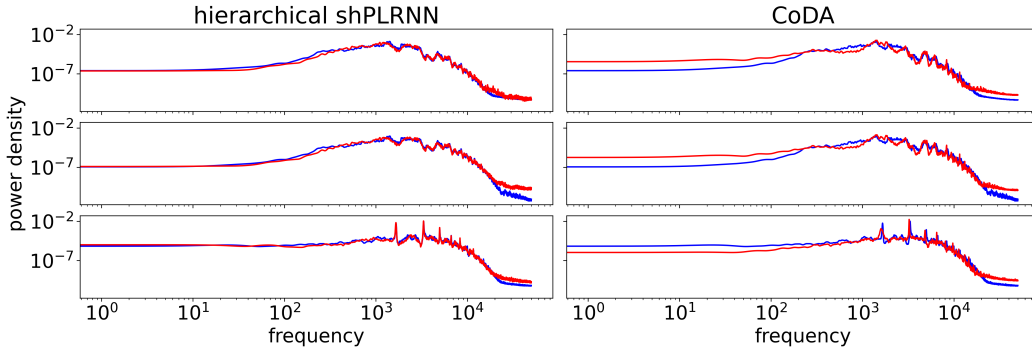


Figure 12: Power spectra of ground truth (blue) and generated (red) trajectories of one of the Lorenz-63 settings for a hierarchical shPLRNN and CoDA.

**ROCKET and MiniRocket** ROCKET (RandOm Convolutional KErnel Transform), and its variant MiniRocket, use random convolutional kernels to project time series into high-dimensional feature spaces useful for linear classification and unsupervised feature extraction (Dempster et al., 2020; 2021). Here we used the default setting of 10,000 random kernels in the `tslearn` package, leading to a 20,000-dimensional embedding space.

**Attention-based Convolutional Autoencoders** Lastly, we trained an attention-based convolutional autoencoder (Wang et al., 2023), alternating convolutional layers with time and feature attention layers in sequential order. We fitted a GMM for unsupervised cluster assignment to the latent representations learned by the encoder, where we chose the size of the encoding space to be the same as that of the hier-shPLRNN feature space ( $N_{\text{feat}} = 10$ ).

Table 5: Average classification accuracy of Gaussian Mixture Models (GMMs) applied to features extracted through various unsupervised methods on the EEG data. Values are across 10 training runs for each model for non-deterministic approaches (hier-shPLRNN, MiniRocket and Attn-Conv-AE), with 10 randomly initialized GMMs evaluated per run.

Model	Classification Accuracy
hier-shPLRNN	<b>92.6 ± 1.2%</b>
ROCKET (Dempster et al., 2020)	71.25 ± 2.2%
MiniRocket (Dempster et al., 2021)	65 ± 13%
tsfresh (Christ et al., 2018)	68.1 ± 3.3%
Catch-22 (Lubba et al., 2019)	57.6 ± 2.5%
Attn-Conv-AE (Wang et al., 2023)	71.5 ± 1.8%

## B FURTHER RESULTS

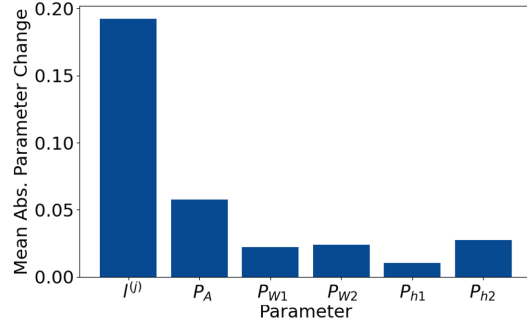


Figure 13: Average parameter changes during training of a hierarchical model on time series of the Lorenz-63 system. Subject-specific feature vectors ( $l^{(j)}$ ) change much more than group-level parameters ( $P_A, P_{W1}, P_{W2}, P_{h1}, P_{h2}$ ).

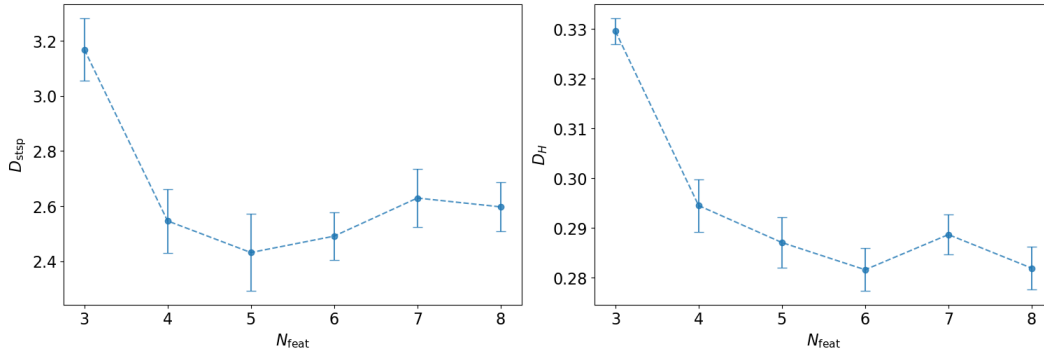


Figure 14: Reconstruction performance as a function of  $N_{\text{feat}}$  for models trained on the 64-subject Lorenz-63 dataset. The feature vector must be large enough to encode the variation in subject-specific dynamics when changing all three of the Lorenz-63 bifurcation parameters (but may not be too large either).

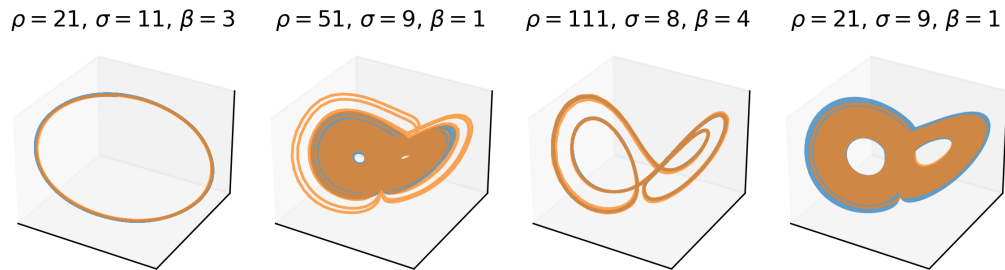


Figure 15: Ground truth (blue) and hier-shPLRNN generated (orange) trajectories for the Lorenz-63 system. Shown are four example parameter combinations, illustrating different dynamical regimes of the system. All of these were generated by the same hier-shPLRNN model.

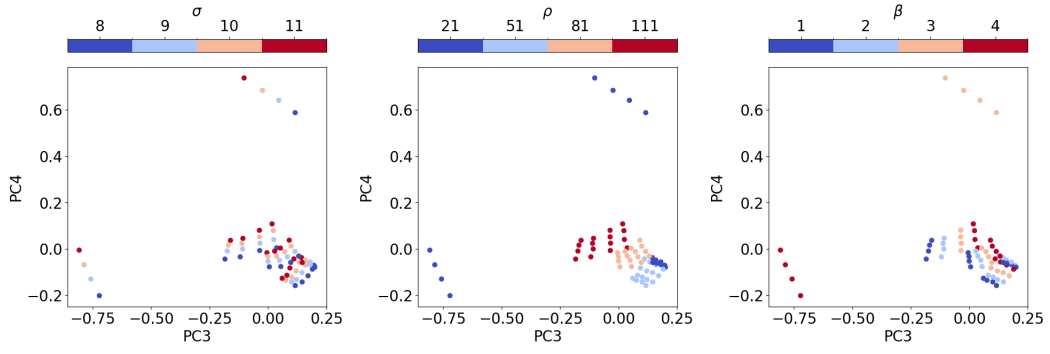


Figure 16: Same as Fig. 3 for the third and fourth principle component.

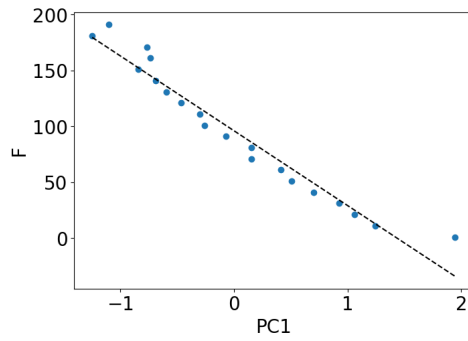


Figure 17: First PC of the 5d feature vector of a hier-shPLRNN, trained on the Lorenz-96 system in Sect. 4.1, aligns with the ground truth forcing parameter  $F$  used to generate the training data.

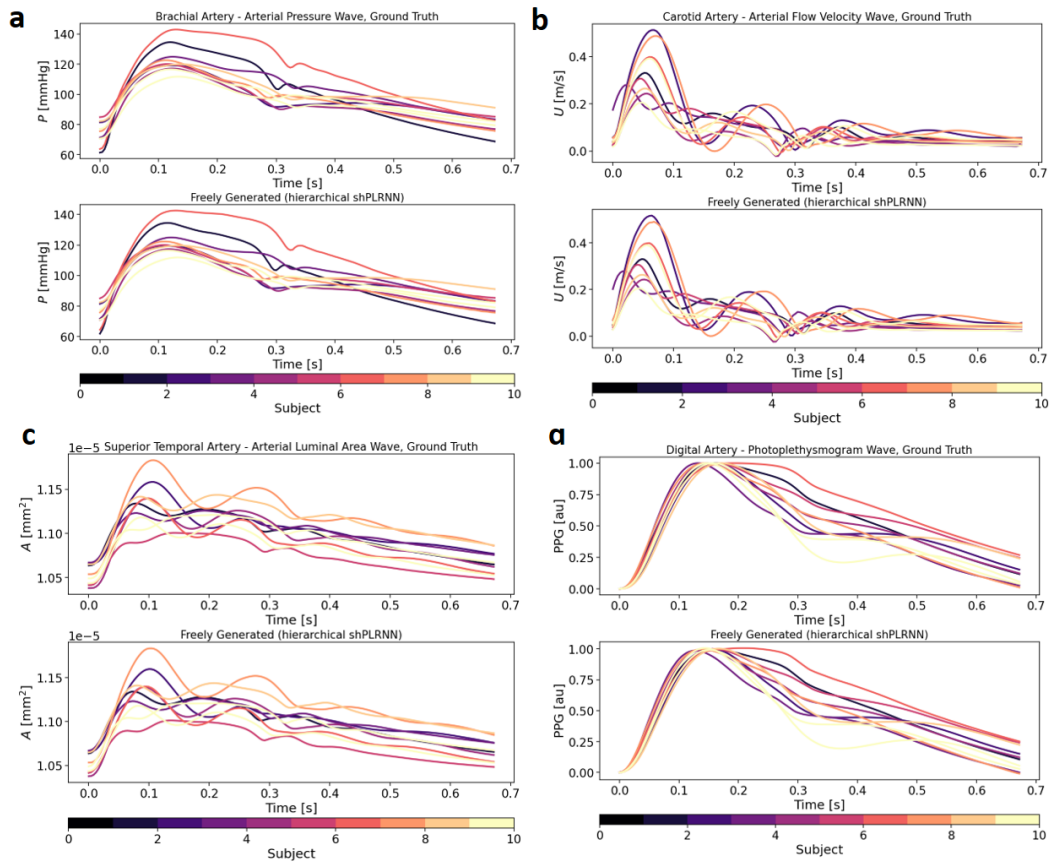


Figure 18: Ground truth and freely generated arterial pressure wave (a), arterial flow velocity wave (b), arterial luminal area wave (c) and photoplethysmogram wave (d), simulated at 4 different anatomical sites, for 10 representative subjects (selected by k-medoids, color-coded).

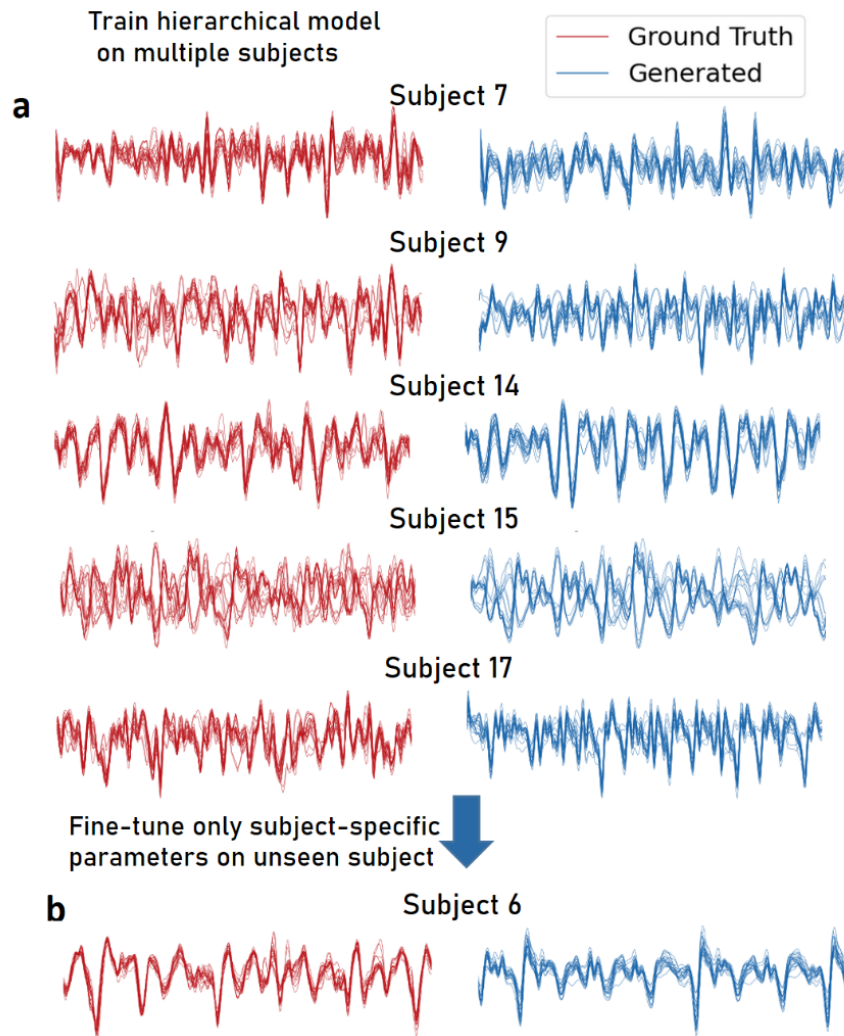


Figure 19: Example reconstructions of several subjects from the experimental fMRI dataset using a hier-shPLRNN with  $N_{\text{feat}} = 10$ ,  $L = 300$ , and training by GTF with  $\alpha = 0.1$ .

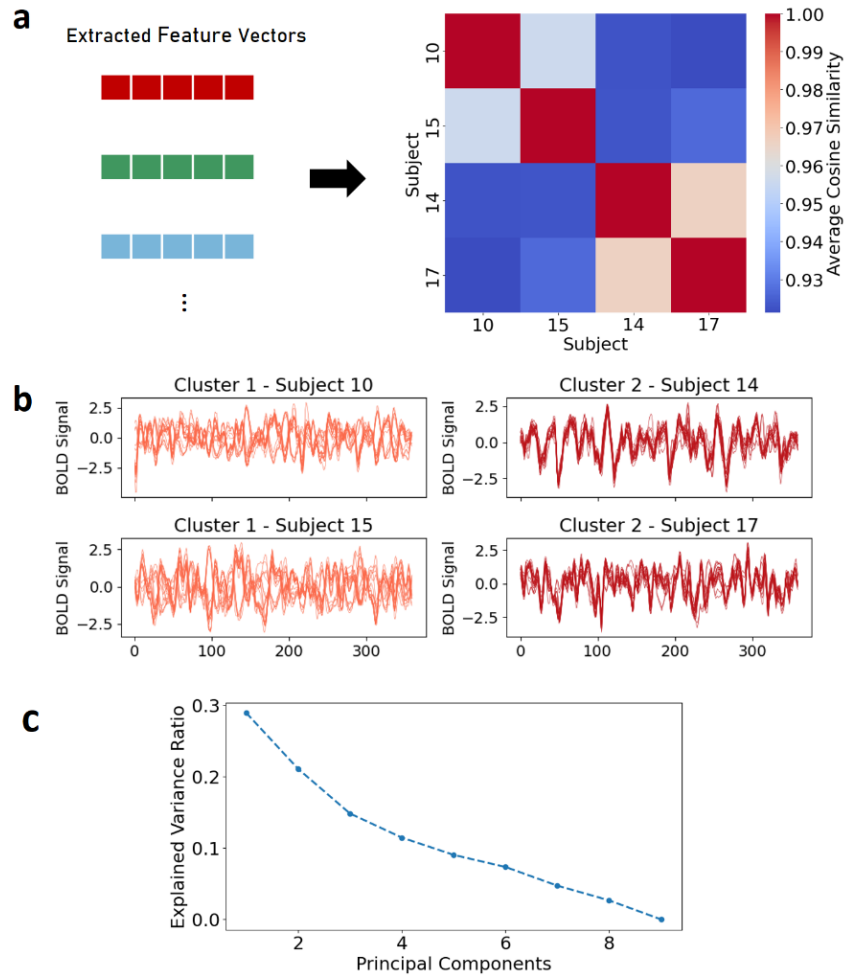


Figure 20: **a**: Cosine similarity matrix based on the average similarity of the feature vectors across 20 training runs for 4 example subjects. **b**: Extracted similarities and cluster labels reflect visual differences in the recorded BOLD signals. Cluster assignments were consistent across all 20 runs for all subjects except one (subject 7), for whom the cluster assignment alternated between both clusters with a 50/50 split. **c**: Explained variance ratio for the principal components obtained from a PCA on the subject feature space for a model trained on the 10 fMRI subjects.